ACS Catalysis

pubs.acs.org/acscatalysis

Perspective

Rigor and Reproducibility in Electrocatalysis: Best Practices for Operando Studies

Brian M. Tackett,* Marcel Schreier, Ezra L. Clark, Evan P. Jahrman,* Linsey C. Seitz, Adam S. Hoffman, Qiaowan Chang, Simon R. Bare, Jingguang G. Chen, Matthias M. Waegele,* Elizabeth R. Corson, Anthony Shoji Hall, Sungin Kim, Jiahong Jiang, Yao Yang,* and David Raciti*

Cite This: https://doi.org/10.1021/acscatal.6c01946

Read Online

ABSTRACT: Operando measurements have rapidly expanded the scope of electrocatalysis by enabling direct observation of catalytic interfaces under working conditions and by linking structural, compositional, and spectroscopic observables to activity and selectivity. However, the growth of operando methods has outpaced the adoption of broadly shared experimental standards, creating persistent challenges in reproducibility, interpretation, and comparison across laboratories and platforms. This perspective synthesizes discussions from the 2025 National Science Foundation Workshop on Rigor and Reproducibility in Electrocatalysis and outlines a practical framework for the rigorous use of operando measurements in electrocatalysis. We highlight three recurring needs: careful implementation of complex methods to avoid overinterpretation; recognition that (subtle) differences in reactor architecture, hydrodynamics, and electrical boundary conditions can alter apparent kinetics and selectivity; and transparent reporting standards that enable meaningful cross- comparison without constraining measurement-specific cell innovation. Focusing on widely used techniques (including X-ray and vibrational spectroscopies, mass spectrometry, and electron microscopy), we discuss technique-specific pitfalls, cross-validation strategies, and recurring platform-agnostic considerations such as mass transport, current distribution, temporal-resolution mismatches, and catalyst evolution. This Perspective aims to strengthen the mechanistic inference and improve the reproducibility, comparability, and predictive value of operando electrocatalysis research.

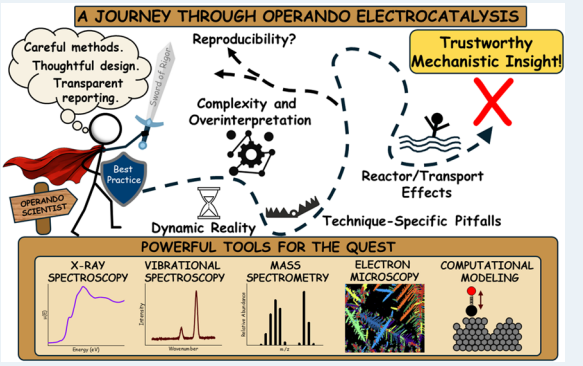

KEYWORDS: *electrocatalysis, operando electrocatalysis, in situ characterization, operando spectroscopy, X-ray absorption spectroscopy, vibrational spectroscopy, electrochemical mass spectrometry, reproducibility*

INTRODUCTION

Over the past decade, electrocatalysis research has been transformed by the rapid expansion of numerous in situ/operando (i.e., operating) metrologies.[1−3] These techniques provide unprecedented access to the dynamic evolution of structure and composition of catalytic interfaces under working conditions, and new insights into how molecular transformations relate to catalytic function. Yet, as operando techniques have proliferated and diversified, their implementation has outpaced the establishment of broadly adopted rigorous experimental standards. As a result, challenges persist in reproducibility, data interpretation, and cross-platform comparability that limit the ability to translate operando observations into broadly validated mechanistic understanding.[4−6]

In 2025, the National Science Foundation Workshop on Rigor and Reproducibility in Electrocatalysis convened domain experts to, in part, identify persistent challenges and community needs surrounding operando measurements. Here, operando measurements are defined correctly as those conducted under working catalytic conditions while directly correlating structural, compositional, or spectroscopic observables with quantitative measures of activity or selectivity, such as current density, product formation rates, or faradaic efficiency. In contrast, in situ measurements are more broadly applied to experiments performed under an applied electrochemical bias or controlled environment that may deviate from reaction conditions (e.g., no substrate, differing mass transport conditions), and/or do not simultaneously verify catalytic turnover or product formation. Workshop discussions produced consensus around

Received: March 12, 2026
Revised: June 24, 2026
Accepted: June 25, 2026

three key themes. First, the rapid expansion of complex operando methods, while uniquely insightful, are susceptible to misinterpretation when not rigorously implemented. Second, different laboratories may produce conflicting results due to subtle differences in experimental design, such as reactor configuration or hydrodynamic environment, which can obscure intrinsic kinetics of an electrocatalytic reaction. Third, enhanced community standards and best practices must be leveraged to reliably compare, validate, and translate operando insights into meaningful advances in energy and chemical technologies. Given the inevitable diversity of operando cell designs driven by measurement-specific innovation, these standards should emphasize rigorous and transparent reporting of experimental configurations, rather than prescriptive standardization of reactor geometries. Detailed documentation of cell architecture, electrode placement, and transport-relevant dimensions, including the use of schematics or digital 3D representations where feasible, would enable meaningful cross-platform comparison and support emerging data-driven and machine learning approaches that rely on well-annotated experimental metadata.

This Perspective synthesizes the workshop outcomes and proposes a holistic framework for operando metrology, centered on widely adopted electrocatalysis techniques, such as X-ray and vibrational spectroscopies, mass spectrometry, and electron microscopy probes, with an emphasis on experimental rigor, cross-validation, and transparent data reporting (with a best practice checklist provided in the Supporting Information). Technique-specific considerations and potential pitfalls are provided to guide experimental design, execution, and interpretation, anchored by established references. This document serves as an open invitation to both new and experienced practitioners to reflect on operando techniques as quantitative measurements so they may be reliably correlated with electrocatalytic performance. An emphasis is placed on recurring cross-platform concerns, such as mass transport, current distribution/electric field, temporal resolution mismatches, and catalyst evolution that demand attention regardless of the technique. Establishing common metrological foundations across diverse operando tools—and intentionally integrating results across modalities—will help transform these techniques from primarily descriptive probes into quantitative, predictive measures of electrocatalytic active sites.

■ CROSS-PLATFORM CHALLENGES

Operando electrocatalytic measurements often require cell designs and methods that deviate from routine laboratory practices to accommodate spectroscopic probes, time-resolved product detection, and microscopic spatial imaging. In this section, we highlight common aspects (Figure 1) across operando measurement platforms that pose challenges to rigorous data interpretation and reproducible results.

Mass-Transport Limitations

Many operando electrochemical cells employ thin electrolyte-layer designs that have large electrode surface area to electrolyte volume ratios. This can induce mass-transport limitations during operation that would otherwise not be encountered in a standard electrochemical cell. Mass transport of reactant species influences the electrochemical measurement when the concentration of that species at the electrode surface differs significantly from that in the bulk electrolyte (Figure 1a). For a steady-state measurement, a calculation of the limiting current density (i.e., complete mass transport control, A m^{-2}) can be made according to: $i_{lim} = \frac{nF}{s}\left(\frac{DC}{\delta}\right)$, where n is the number of electrons involved in the reaction, F is Faraday's constant, s is the stoichiometric coefficient of the reactant, D is its diffusivity (m^2 s^{-1}), C_∞ is its bulk concentration (mol m^{-3}) and δ is the concentration boundary layer thickness (m). For a flowing electrolyte, δ can be estimated based upon the geometry and hydrodynamics of the system—for example, it should be ≈10× smaller than the hydrodynamic boundary layer formed by fluid flow,[8,9] or the ratio of D/δ can be estimated from correlations of system physical properties, like the Sherwood number.[10] In quiescent electrolyte, the thickness of the electrolyte in the thin-layer cell can be used as the upper limit of δ, although it will typically be smaller if there is a sufficient reservoir of electrolyte/reactant connected to the thin layer. For non-steady-state measurements, the concentration boundary layer will grow with time as $\delta \approx \sqrt{Dt}$. In general, if intrinsic kinetic measurements are desired, experiments are commonly designed to operate at currents not to exceed ≈10% of the limiting current density, a widely used heuristic corresponding to <10% reactant depletion at the electrode surface. Operation beyond this regime introduces increasing mass-transport coupling and requires explicit modeling or correction. If such operation cannot be achieved or is not desired, non-uniformities should be considered and explicitly reported in catalyst performance analysis. The same considerations apply for local pH changes (in which H^+/OH^- are generated or consumed at the electrode) that can alter reaction mechanisms and kinetics, but there are homogeneous buffer reactions to consider when determining such pH gradients and can be employed to account for and interpret substantial pH gradients. There is a need to clearly define the local pH under operating conditions, and understand its impact on catalytic behavior to meaningfully interpret electrochemical performance.

Current Distribution

The local current density at an electrode surface can vary significantly due to geometric configuration (discussed in the "Auxiliary Electrode Choice/Position section"), fluid flow, and electrode resistivity (Figure 1b).[7,11] If concentration gradients can be neglected, the degree of current uniformity can be estimated by the ratio of charge transfer resistance (R_{CT}) to ohmic resistance (R_Ω), sometimes called the Wagner number $\left(Wa = \frac{R_{CT}}{R_\Omega}\right)$.[12,13] R_{CT} is determined as the inverse slope of the polarization curve for the electrochemical reaction of interest or via electrochemical impedance spectroscopy (EIS), and R_Ω is the characteristic length of the electrochemical system (sometimes the electrode radius) divided by electrolyte conductivity. If Wa is much smaller than 1, the current distribution will be very non-uniform. Greater uniformity can generally be achieved with more conductive electrolytes, smaller electrodes, and smaller current densities. If concentration gradients cannot be neglected, the fluid flow can induce further non-uniformities, often with higher local currents at the leading edge of the electrode with respect to the direction of fluid flow. Lastly, if a thin layer electrode is deposited on a less-conductive substrate (such as in some preparations of attenuated total reflection surface-enhanced infrared absorption spectroscopy (ATR-SEIRAS) electrodes on silicon), the current density will tend to be higher near the current collector. This can be mitigated by increasing

https://doi.org/10.1021/acscatal.6c01946
ACS Catal. XXXX, XXX, XXX–XXX

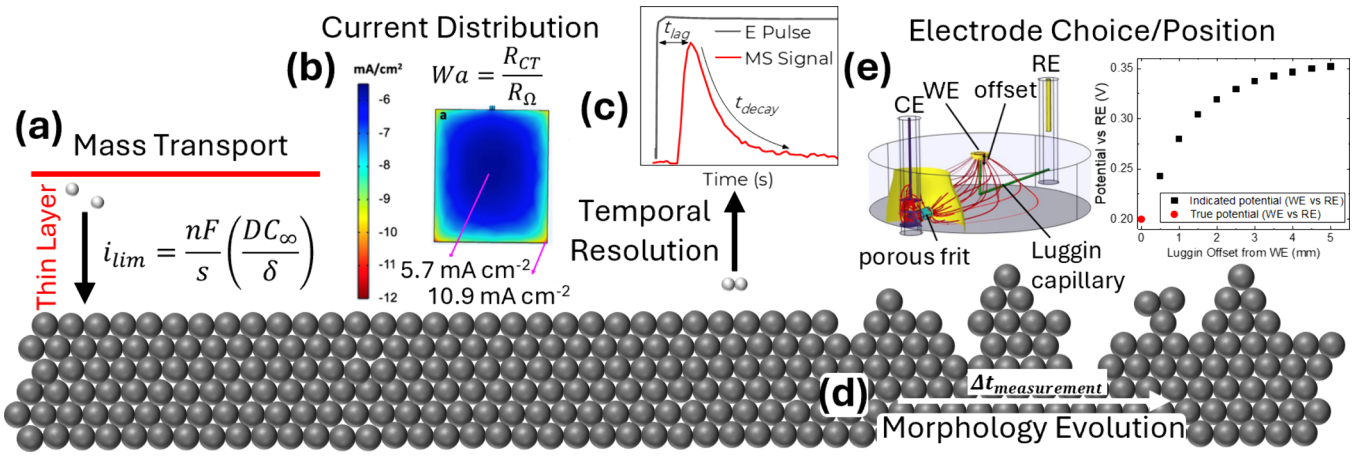

Figure 1. Graphic depicting best practice considerations for electrocatalytic measurements in operando cells. Considerations such as, (a) mass transport conditions, (b) current distribution over the electrode surface, (c) temporal resolution of the measurement, (d) electrode morphology over the duration of the measurement, and (e) relative positioning of (and choice of auxiliary) electrodes.[5] (b) reproduced from ref 7. Copyright 2024 American Chemical Society. (e) Adapted from ref 5. Available under a CC BY 4.0 license (https://creativecommons.org/licenses/by/4.0/deed.en). Copyright 2022 G. Smith and E. J. F. Dickenson.

the metal film thickness to increase total electrode conductivity or decreasing length to the current collector. In a similar vein, because the resistances of operando cells often exceed those of standard electrochemical cells, explicit characterization and reporting of uncompensated resistance (*iR* drop) is critical. Rigorous measurements should provide both measured and *iR*-corrected potentials, along with a description of the compensation protocol used, recognizing that such corrections typically account for a lumped series resistance and may not capture spatial variations in potential across the working electrode in non-uniform or confined operando geometries.

Temporal Resolution

Electrochemical signal responses (current, potential, charge) are orders of magnitude faster than typical operando measurements, which create an inherent challenge for temporally syncing the electrochemical event to its corresponding operando signal (Figure 1c). The nature of this mismatch changes depending on the cell design and the measurements being made, with some having more complex time delay than others—for example, mass spectrometer signal detection depends on species mass transport through various phases. Rigorous data reporting therefore calls for explicit description of the synchronization protocol used for any given measurement.

Catalyst Morphological Evolution

The collection time for certain operando measurements may exceed that of a standard electrocatalytic measurement, which could result in morphological changes to the catalyst under operando conditions that would not otherwise be observed (Figure 1d). To properly attribute catalyst function to a steady-state structural ensemble under operating conditions—recognizing that this ensemble may be dynamic or fluxional—good practice is to assess reversibility and repeatability of the operando measurement. For example, if measurements are made during a series of monotonically increasing potential steps, the reversibility can be tested by making the same measurements during the descending series of potential steps. Alternatively, measurements can return to a reference state between potential steps. Reproducibility can be assessed by repeating this process again, however, this can be logistically difficult for synchrotron-based measurements due to the limited availability of beamtime.

Auxiliary Electrode Choice/Position

The selection and configuration of auxiliary electrodes (both reference and counter) are central to establishing rigorous potential control, current distribution and ensuring artifact-free interpretation of operando results (Figure 1e).[5,14] The relative placement of the auxiliary electrodes is the first consideration for understanding current distribution and the measured electrode potential. In general, the reference electrode sensing point should be positioned as close as feasible to the working electrode to minimize uncompensated resistance, often using a Luggin–Haber capillary where compatible with the operando probe (e.g., not blocking the beam in spectroscopic/e-beam measurements). At the same time, the reference geometry should avoid shielding the electric field or disturbing local mass transport near the measurement region.

A conventional reference electrode with a stable and chemically compatible junction should typically be preferred to an internal pseudo-reference. However, even conventional reference electrodes that perform reliably in standard electrochemical cells can behave unpredictably when incorporated into specialized operando geometries, sometimes even requiring capacitors[15] between the counter and reference to stabilize the electrochemical signal (e.g., when referencing working electrodes in thin resistive channels). Additionally, reference-electrode selection should therefore be dictated jointly by electrolyte compatibility and cell geometry: for example, chloride-containing references are convenient but may be inappropriate when chloride can poison the catalyst, alter dissolution equilibria, or drift under alkaline exposure. A primary example are commercial Ag/AgCl electrodes, many of which have ceramic frits for the junction. Though widely used, these particular electrodes are prone to frit dissolution in hydroxide and to chemical drift arising from AgO/AgCl equilibria when hydroxide enters the reference compartment, leading to systematic shifts in the

https://doi.org/10.1021/acscatal.6c01946
ACS Catal. XXXX, XXX, XXX–XXX

reference potential that may exceed the magnitude of subtle spectral or structural changes under study.[14,16] These effects underscore the importance of explicitly verifying reference stability and conducting routine calibration against appropriate and well-defined redox couples (e.g., Pt–H underpotential deposition, Cu^{2+}/Cu, or ferri/ferrocyanide) throughout an experiment to monitor long-term drift and contamination.[5,14,17,18] Liquid-junction potentials, which can be substantial in non-standard electrolytes or confined geometries, should be estimated or reported when relevant, as they add tens of millivolts of uncertainty to the applied potential.[19] In many custom operando cells, spatial constraints necessitate the use of internal pseudo-reference electrodes (e.g., Pt, Au, Ag wires), but these systems are not true references: their potentials are sensitive to preparation conditions, electrolyte composition, and electrochemical cycling, and can drift by >100 mV during extended measurements.[20−22] Thus, pseudo-references require pre- and post-experiment calibration and must be treated as approximate indicators rather than absolute potential scales. Furthermore, their composition, placement, calibration protocol, and drift should be reported explicitly.

Counter electrodes warrant equal scrutiny. Decreasing the counter–working separation can reduce ohmic loss and enable higher accessible current densities, but it may also exacerbate non-uniform current distribution and increase the likelihood that species generated at the counter electrode reach the working electrode. Even trace amounts of dissolved species crossing from the counter to the working compartment can alter catalytic pathways, poison reactive sites, or introduce spurious features in operando X-ray absorption and vibrational spectra. Pt counter electrodes, in particular, are known to undergo trace dissolution, leading to solution-phase Pt concentrations at the sub-nanomolar level that can redeposit on the working electrode surface, yielding vibrational signatures that are easily misassigned to intrinsic catalyst behavior.[23] Such crossover can occur even in cells with modest hydrodynamic coupling, emphasizing the need for careful physical separation of the counter electrode via salt bridges, ion-exchange membranes, or flow-separated architectures. When possible, chemically defined counter electrodes—such as graphite, glassy carbon, or noble metal coated Ti mesh—should be used to minimize contamination pathways. Ultimately, the unusual geometries of operando cells can also exacerbate potential gradients along the working electrode or between the working and reference electrodes, reinforcing the principle that operando cell design must be organized around the perturbation of current flow. Collectively, careful selection, calibration, isolation, and documentation of reference and counter electrodes are essential for achieving reproducible potential control and avoiding parasitic processes that can propagate through all operando measurement platforms.

Probe/Beam Effects

Techniques that involve X-ray or electron probes are inherently subject to beam-induced damage that can artificially influence measurements. In X-ray and electron microscope-based operando studies, irradiation can alter the electronic structure of catalysts, drive unintended redox processes, or promote the formation of reactive species in the electrolyte. As a result, rapid or repeated scans, and/or sampling new areas of the electrode, and comparative beam-off studies are often required to identify unexpected spectral evolution and to distinguish intrinsic electrochemical changes from probe-induced effects. It is therefore prudent to monitor electrochemical performance and product formation for deviations that correlate with beam exposure, as identified in comparative beam-off studies, or that depart from behavior observed in conventional benchtop cells. If materials are found to be radiation sensitive, an appropriate mitigation strategy should be implemented. Many strategies exist, including minimizing the dose a region on the sample receives by defocusing the beam or frequently translating to fresh regions on the sample. Alternatively, changes to the environment may be needed, such as leveraging electrolyte flow to flush radicals away from the electrocatalyst's surface,[24] minimize local heating, or lower liquid temperature to suppress beam damage.[25−28] As the cause and severity of beam-induced damage depends strongly on the measurements and materials in a given study, testing and consideration is required to select the optimal mitigations. Once selected, the mitigation strategy should be reported with sufficient detail to evaluate its effectiveness.

Importantly, beam effects are not limited to high-energy probes. Although vibrational spectroscopies employ lower-energy photons, intense optical fields can still perturb the electrochemical interface through localized heating, plasmonic enhancement, photochemical reactions, or laser-induced adsorption and desorption processes.[29−31] Such effects may lead to apparent potential-dependent spectral features that do not reflect intrinsic interfacial chemistry. Consequently, operando vibrational measurements similarly require control experiments, including variation of laser power density, beam position, and exposure time, to establish that observed spectral changes are not probe-induced artifacts.

Device-Level Architecture

As electrocatalysis moves toward device-relevant architectures (e.g., membrane electrode assemblies and zero-gap cells) the cross-platform considerations discussed become increasingly important. In these systems the factors governing current distribution, transport, and interfacial chemistry are more convolved, being influenced by parameters such as the membrane/ionomer phase, porous transport layers, feed humidification, and flow-field design. Consequently, liquid-water management, gas crossover, salt precipitation or flooding, and local pressure gradients can strongly influence the device's performance under practically relevant operating conditions. Operando measurements are especially valuable in this context because these architectures create environments most relevant to industrial relevant performance; however, that same complexity makes robust interrogation more challenging. For example, optical probes can be challenged by backside gas channels, membrane-backed catalyst layers, and ionomer-covered porous electrodes that restrict line-of-sight access and preclude measurement configurations commonly used in liquid-phase cells. As a result, specialized cell designs are often required that enable alternative illumination geometries or more optically accessible current-collector architectures.[32] A full discussion of the many practical device configurations is beyond the scope of this Perspective. Readers are directed to recent reviews for more information.[33−36] The central principle, however, remains unchanged: if a measurement is to be considered truly operando, the integrity of the device-level electrochemical configuration should be preserved and the methods

https://doi.org/10.1021/acscatal.6c01946
ACS Catal. XXXX, XXX, XXX−XXX

employed to perform the operando measurement should be thoroughly reported.

■ TECHNIQUE-SPECIFIC CONSIDERATIONS

X-ray Absorption Spectroscopy

The information accessible to a particular X-ray absorption spectroscopy (XAS) method determines where and how it can be rigorously applied. Soft X-rays ($\lesssim$2 keV) often reveal the chemistry of adsorbates/electrolytes, and/or the electronic structure of catalytically relevant metals. This information is elucidated by the near-edge X-ray absorption fine structure (NEXAFS) of K-edges of light elements (e.g., C, O, N) and L-edges of first-row transition metals dominated by 2p–3d transitions.[37−40] Hard X-rays ($\gtrsim$4.5 keV) can probe transition metal K- or L-edges, see Figure 2a. Hard X-ray absorption spectra are partitioned between the X-ray absorption near-edge structure (XANES) and extended X-ray absorption fine structure (EXAFS) to survey electronic and atomic structure,

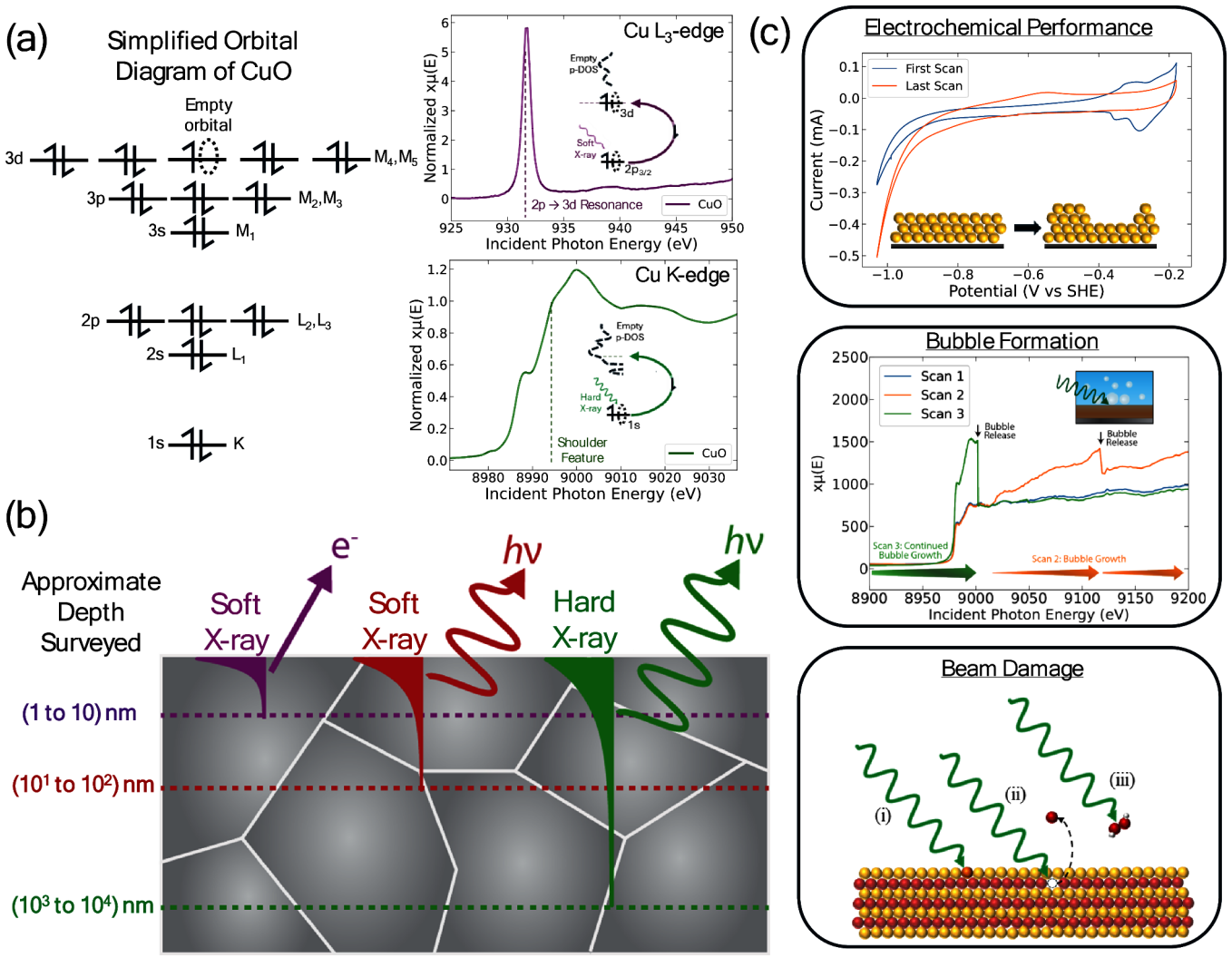

Figure 2. (a) Depiction of states often probed by XAS, including a simplified orbital diagram for CuO and the unoccupied partial density of states (p-DOS) accessible to a dipole transition. Example data show (top) soft XAS in total electron yield demonstrating the sharp resonance features observed when direct 2p–3d transitions are accessible, and (bottom) hard XAS collected in transmission. (b) Nominal information depths for soft XAS collected by detecting electrons or fluorescence and for hard XAS via fluorescence. The precise information depth depends on compositions, photon energies, incident and exit angles, and which electrons are collected (i.e., Auger, secondary, and/or photoelectrons).[45] Reproduced from ref 44. Copyright 2024 American Chemical Society. (c) Three topics that require persistent monitoring: (Top) cyclic voltammetry curves for a Cu(111)/Si(110) catalyst corresponding to the first and last XAS scans in an experiment. The CV curves reveal catalyst restructuring. It is prudent to constantly monitor electrochemical data for unexpected or evolving results. (Middle) XAS data collected via fluorescence with the incident beam well-below the critical angle to limit bulk penetration. The copper sample was in KOH solution at sufficiently negative potentials to generate gaseous products. The second scan shows a gradually higher fluorescence signal above 9000 eV as bubbles disrupt the optical path. Bubble accumulation, and gradually increasing signal, persists until a similar energy in the third scan. The discontinuities in the second scan at 9125 eV and in the third scan at 9000 eV are due to bubbles releasing from the surface. Notably, during back illumination of catalysts on gas diffusion layers, bubbles can decrease fluorescence signals if absorbing gases like argon are used. (Bottom) While the specifics of beam damage vary,[60] three mechanisms are shown for a metal oxide catalyst, including (i) photoreduction/oxidation, (ii) defect formation (which can be related to photoreduction/oxidation),[61] and (iii) radical or peroxide formation in the electrolyte.

https://doi.org/10.1021/acscatal.6c01946
ACS Catal. XXXX, XXX, XXX−XXX

respectively.[41] Results from XANES or EXAFS can bolster interpretation of the other. For example, oxides, hydroxides and oxyhydroxides may have similar features in their XANES spectra, yet detailed EXAFS modeling can break this ambiguity through comparison of fitted scattering path lengths and coordination (notably the first metal–O path(s)) to the bulk crystal structures. Moreover, complementary soft and hard X-ray measurements strengthen structural assignments of complex active sites, and measurements surveying the edges of multiple elements probe complementary cation/anion pairings.[42−44]

Thoughtful sample preparation tailored to the specific measurement is also critical. For soft X-rays, absorption is frequently measured indirectly by collecting emitted photons (fluorescence), the photoelectric current, or emitted Auger electrons.[45] For hard X-rays, spectra are often collected in transmission or fluorescence yield. Notably, the latter is preferred for samples that are dilute or thin compared to the attenuation length of the material,[41] and also for operando studies in which cell components and electrolytes prevent transmission of X-rays.[46] Soft and hard X-ray studies encounter similar sample preparation challenges. Transmission experiments require samples to be homogeneous in thickness, free of pinholes, and of appropriate particle size.[49] Especially absorbing samples can disproportionately transmit high-energy harmonics or show spectral distortions.[50,51] Likewise, concentrated fluorescence samples exhibit "self-absorption", resulting in a nonlinear relationship between the fluorescence intensity and absorption coefficient. When possible, it is preferable to prepare samples so that self-absorption is negligible. Otherwise, spectra require corrections that may be particularly sensitive to the sample's composition, the experimental geometry, or other approximations.[43,52−55] Fluorescence measurements should also consider whether the entire system under study contains elements with competing fluorescence lines and whether the detector has sufficient energy-resolution to isolate the fluorescence of interest.[56] Finally, electron yield measurements in operando studies are complicated by the need to facilitate the escape of weakly-penetrating electrons.

The operando aspect of electrochemical XAS studies imposes several additional challenges. First, soft X-ray studies in vacuum chambers need robust cells free of leaks or window defects to maintain the integrity of the beamline and minimize in-air cell adjustments; successful designs are available.[57,58] Second, experiments should be monitored for electrochemical performance matching expectations (Figure 2b). Notably, it is best practice to verify that electrochemical performance in the XAS cell is consistent with a standard electrochemical cell in the researcher's laboratory prior to the experiment. Third, it is often necessary to monitor bubble formation, especially for gas-evolving reactions at large overpotentials, as any disruption of the optical path can distort experimental spectra. Two common mitigations are the use of faster acquisition rates that allow for isolating periods without bubbles and/or implementing cell designs that rapidly sweep bubbles away.[3,59] Experiments should also be monitored for unexpected spectral changes from beam damage.[60,61] Similarly, unnormalized spectra (i.e., before pre- and post-edge normalization) should be monitored for changes in the magnitude of the edge step, a function of the amount of the measured element,[40] to identify potential metal dissolution. Finally, operando XAS studies should use cells enabling appropriate mass transport.[3] Indeed, consistent mass transport control and sample preparation are also essential to studies pairing non-simultaneous measurements across complementary techniques, with beamlines spanning the edges/spectroscopies of interest offering one solution.[47,48]

When analyzing operando XAS measurements of electrocatalysts, interpretations should take into account how rapidly the measurement is performed, how deeply into the material the X-rays probe, and how rigorously the findings can be verified via simulations. First, traditional step-scanning XAS beamlines often require several minutes to collect a spectrum, but fly-scanning, high-flux beamlines enable sub-minute acquisition rates, and beamlines equipped with a specialized quick-scanning monochromator enable millisecond temporal resolution.[62] This enables close monitoring of catalyst reconstruction and evolution, with the caveat that measurements still reflect the volume- and time-weighted average of chemical species within the illuminated region. As a result, spectators can still mask transient species unless a perturbation is leveraged, such as in modulation excitation spectroscopy.[63,64] Second, Figure 2c stresses the attenuation lengths typical of different energy regimes and measurement modes and highlights that choices typically extend well past the surface processes of interest. Nanoparticles are often employed to enhance interfacial phenomena, however the associated XANES spectra often differ from the corresponding bulk counterparts.[65] Such spectral differences can highlight the unique electronic structure assumed by a nanomaterial, but complicate interpretations relying on bulk empirical standards. In such instances, theoretical simulations can be particularly useful in interpreting the spectra of interest. Third, DFT modeling is often needed to confirm the presence/absence of species associated with a proposed mechanism, a valuable piece of information for kinetic models.[66] Codes such as NWChem and OCEAN can calculate XAS spectra of anticipated structures to compare hypotheses with experimental results.[67,68] Alternatively, researchers can test hypotheses by estimating parameters relevant to coordination chemistry.[69] In particular, CTM4XAS allows users to tune crystal-field and charge-transfer parameters to reproduce XAS spectra,[70] and the bond lengths and coordination numbers corresponding to FEFF-calculated scattering paths can be fit to EXAFS data.[71] Beyond the information covered here, a discussion on the limitations of XAS analysis can also be found in a recent perspective focusing on thermal catalysis.[72] There, recommendations can be found on evaluating signal-to-noise in XAFS data, constructing EXAFS models beyond the first coordination shell, and best practices for data reporting, which may serve as a useful supplement to the present article for interested readers.

Vibrational Spectroscopy (Raman/IR/SHINERS/SFG)

While operando X-ray spectroscopies provide powerful insight into catalyst coordination environments and oxidation states, researchers often employ more accessible vibrational spectroscopies to probe the molecular-level structure of interfacial species central to electrocatalytic mechanisms. Vibrational spectroscopies, such as infrared, Raman, and nonlinear optical probes (e.g., sum-frequency generation (SFG))[73−75] provide molecular-level details of the electrochemical interface and nearby electrolyte, including the identities and configurations of adsorbates, reaction intermediates, and solvent species. Whereas SFG is intrinsically interface-selective due to the absence of inversion symmetry at interfaces, surface-enhanced

https://doi.org/10.1021/acscatal.6c01946
ACS Catal. XXXX, XXX, XXX−XXX

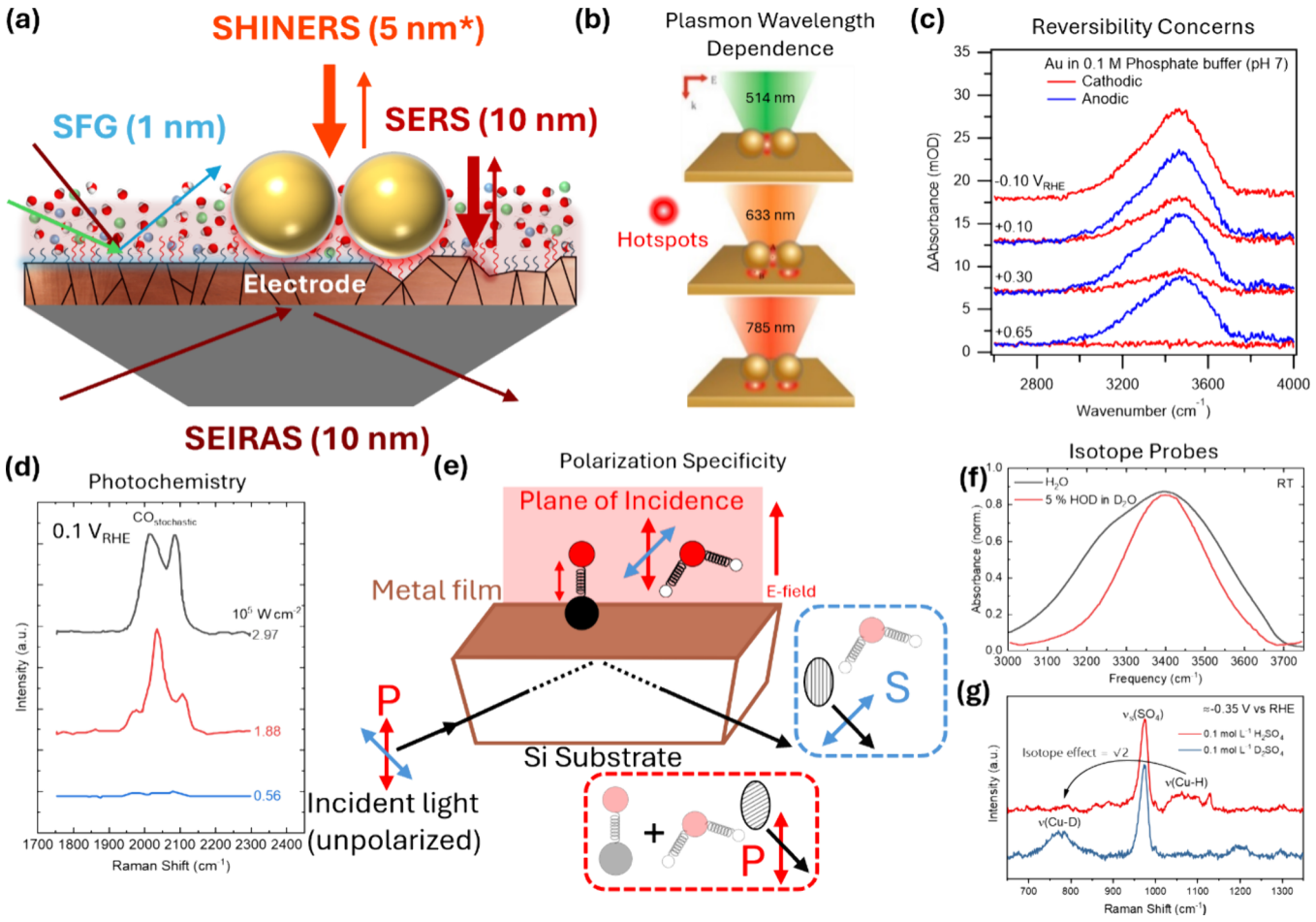

Figure 3. (a) Schematic depicting sum-frequency generation (SFG), surface-enhanced infrared absorption spectroscopy (SEIRAS), shell-isolated nanoparticle-enhanced Raman spectroscopy (SHINERS), and surface-enhanced Raman spectroscopy (SERS) including approximations of the length scale of vibrational information reported. (*) The "hotspot" or plasmonic response of the particle used in SHINERS is a tunable parameter (e.g., size of the particle, laser wavelength). (b) Schematic depicting the dependence of electric field (hot spots) as a function of wavelength used. Reproduced from ref 77. Copyright 2016 American Chemical Society. (c) ATR-SEIRA spectra showing the irreversibility of the ν(O–H) of interfacial water collected using a Au electrode in 0.1 mol L^{-1} phosphate buffer (pH 7).[88] Reproduced from ref 88. Copyright 2026 American Chemical Society. (d) Raman spectra depicting photoinduced CO adsorption to a Cu surface as a function of laser dose at 0.1 V versus the reversible hydrogen electrode (RHE). Reproduced from ref 29. Copyright 2025 American Chemical Society. (e) Schematic demonstrating use of polarization to determine surface adsorbate vibrational bands and electrolyte vibrational bands. Isotopic experiments to study (f) water structure[96] or (g) surface hydride formation on Cu(111).[97] (f) is reproduced from ref 96. Copyright 2016 American Chemical Society. (g) is reproduced from ref 97, Copyright 2021 American Chemical Society.

methods such as SEIRAS,[76] surface-enhanced Raman spectroscopy (SERS), and shell-isolated nanoparticle-enhanced Raman spectroscopy (SHINERS) achieve sensitivity through plasmonic or field-enhancement effects that amplify signals from surface or near-surface species. Together, these techniques bridge a wide range of probing depths—from a few molecular layers in SFG to tens of nanometers in SEIRAS (Figure 3a)—providing a continuum of information that is invaluable, but also challenging to interpret. The same sensitivity that makes these tools indispensable also renders them particularly vulnerable to artifacts arising from optical coupling[77,78] (Figure 3a,b), electrode morphology, and the strong vibrational response of the surrounding electrolyte.

A key challenge to rigor and reproducibility in operando vibrational spectroscopy lies in defining what portion of the signal truly reflects the interfacial/surface events of interest, rather than contributions from spectator species or the bulk electrolyte. In SEIRAS, for example, the penetration depth of the evanescent field (≈5 to 100 nm) exceeds the typical width of the electrochemical double layer by one to two orders of magnitude (Figure 3a).[79,80] Observable peaks and their lineshapes sensitively depend on the properties of the thin film electrode.[81,82] Consequently, even subtle changes in the electrode–electrolyte interface (arising from surface reconstruction, nanostructuring, local pH drift, or gas evolution) can complicate subtraction of bulk solvent contributions, producing potential-dependent spectral features whose interfacial versus solution-phase origins must be carefully disentangled (Figure 3c). Likewise, in Raman spectroscopy, fluorescence background, laser induced heating, and photoinduced chemistry can distort both intensities and frequencies.[30,31,83−85] Indeed, laser-induced adsorption events (e.g., stochastic CO adsorption on Cu) have been directly observed in operando Raman measurements and were only identified as artifacts through

https://doi.org/10.1021/acscatal.6c01946
ACS Catal. XXXX, XXX, XXX−XXX

complementary SERS and SEIRAS performed in the same electrochemical cell (Figure 3d).[29]

These effects underscore the necessity of rigorous control experiments—such as isotopic substitution, potential cycling to assess reversibility, alternating potential sequences to test for hysteresis, and direct comparison of catalyst-coated and bare substrates—to discriminate true interfacial chemistry (particularly weak or emergent bands) from extrinsic perturbations of the optical or electrochemical environment (e.g., dipole–dipole interactions).[86−89] Such effects are well established for surface-adsorbed CO, where dynamical dipole coupling and intensity borrowing can break simple relationships between band area and coverage.[90,91] Furthermore, discriminating vibrational bands associated with surface-adsorbed species from an evolving spectral background (arising from bulk and interfacial solvent vibrations, refractive-index changes, and field-induced intensity variations that evolve with applied potential) remains central to the reliable interpretation of operando vibrational spectra. Under simple circumstances adsorbed species can be directly distinguished from dissolved species (e.g., ATR-SEIRAS and adsorbed/dissolved carbonates),[92] however this still requires explicit measurement of solution reference spectra and transparent reporting of electrode activation protocols and stability, including electrochemical conditioning procedures and the temporal persistence of the catalytic surface under operando conditions.

An adsorption band attributable to a surface-bound species reflects a discrete vibrational mode with well-defined frequency and symmetry, typically exhibiting characteristic isotope shifts, polarization dependence, or reproducible potential dependence, whereas background contributions often arise from bulk solvent responses that vary with refractive index, solvation environment, or interfacial pH, all of which can evolve with applied potential. These background variations are frequently misinterpreted as interfacial chemistry even in the absence of surface adsorbates. Polarization-dependent measurements can provide useful constraints for vibrational band assignment; however, their interpretation depends on the specific cell/electrode geometry and local field distribution. For example, in many thin-film SEIRAS configurations, p-polarized light preferentially couples to surface-normal components of transition dipole moments and is therefore often used to enhance sensitivity to interfacial species, while s-polarized light can be more strongly influenced by bulk electrolyte contributions (Figure 3e).[93,94] Direct comparison of s- and p-polarized spectra can thus aid discrimination between interfacial and solution-phase responses. Nevertheless, this distinction is not universal: for certain SEIRA-active film morphologies or field distributions, s-polarized light can also yield strong signals from surface-adsorbed species.[95] Accordingly, polarization dependence should be interpreted as a supporting diagnostic rather than a definitive criterion, and is most powerful when combined with strategies discussed in the preceding paragraph.

Isotopic dilution of H_2O provides one of the clearest demonstrations of how vibrational coupling and solvent background can confound interpretation (Figure 3f).[96] SEIRAS studies performed in isotopically dilute electrolytes have produced fundamentally different conclusions regarding interfacial water structure compared with conventional H_2O electrolytes, revealing the dominant role of intra- and intermolecular vibrational coupling in shaping observed spectra.[98] Similarly, SFG measurements at the air–water interface show that both inter- and intramolecular coupling strongly influence spectral line shapes and intensities, effects that can be minimized through isotopic dilution.[99] Often, vibrational coupling effects are also present in other systems involving a (locally) high density of oscillators with significant oscillator strength, surface-adsorbed CO being a prominent example. Here, dynamical dipole coupling can affect peak frequencies and break linear scaling between total peak area and surface coverage.[91,100]

Quantitative comparison of vibrational intensities across materials presents an additional challenge. Researchers frequently compare integrated band intensities in SEIRAS, SERS, and SHINERS as proxies for relative surface coverage. However, plasmonic enhancement factors are acutely sensitive to local nanostructure, composition, and morphology, and even modest compositional changes in alloys or supports can strongly alter enhancement efficiency. Consequently, direct comparison of integrated band intensities can be rendered effectively meaningless unless enhancement factors are independently constrained. Such comparisons must therefore be approached with caution and supported by complementary normalization strategies or independent surface coverage measurements. Interpretation of absolute intensity is particularly fraught in vibrationally resonant-SFG due to the heterodyne nature of the signal and the strong dependence of the non-resonant background on local field/potential via electric-field induced second harmonic generation (EFISH) like mixing. Proper spectral fitting,[101] heterodyne detection,[102] and/or non-resonant background suppression[103] techniques should be used.

Reproducibility also depends critically on transparent reporting of optical and electrochemical parameters. Robust optical alignment, calibration of the wavenumber and intensity scales, and explicit quantification of laser power density at the electrode surface are essential for meaningful cross-comparison between laboratories. When enhancement effects are exploited, reproducibility must also be demonstrated across independent substrates and over extended cycling (or time), as nanostructured plasmonic surfaces may undergo electrochemical restructuring (Figure 3c).[88] Reporting the synthesis history, morphology, and electrochemical conditioning of SERS and SEIRAS substrates—together with verification that observed signals originate from the catalyst rather than the support—substantially strengthens interpretability. Complementary validation through isotope labeling[97] (Figure 3g), differential capacitance measurements, spectral normalization, or comparison with simulated spectra further mitigates ambiguities associated with solvent and co-adsorbate contributions, thereby strengthening the quantitative interpretation of operando vibrational methods as probes of interfacial chemistry enabling more robust discrimination between specific surface species and broader, correlative spectral changes.[104−106]

Finally, a coordinated effort to establish open, community-curated spectral databases would significantly advance reproducibility and mechanistic consensus in the field. Existing repositories such as the National Institute of Standards and Technology (NIST) Chemistry WebBook (https://webbook.nist.gov/chemistry/) and the RRUFF* Raman database (https://www.rruff.net/) provide valuable reference spectra for molecular systems, but lack data acquired under electrochemical conditions. A dedicated community database for in situ and operando spectra collected in well-defined

https://doi.org/10.1021/acscatal.6c01946
ACS Catal. XXXX, XXX, XXX−XXX

electrochemical environments, with parameter tabulation, would enable systematic cross-validation of both experimental and computational assignments promoting reproducibility and comparability across laboratories.

Mass Spectrometry (EC-MS/DEMS)

Although X-ray and vibrational methods can probe catalysts under electrochemical bias, their interpretation as operando measurements is most rigorous when paired with product-resolved detection that directly links structural or spectroscopic observables to catalytic turnover. Mass spectrometry contributes as a leading tool to link structural and interfacial signatures to quantitative partial currents and product formation in real time. Electrochemical mass spectrometry (EC-MS), or differential electrochemical mass spectrometry (DEMS), enables sensitive and rapid detection of volatile species evolved or otherwise generated at an electrode under operando conditions (Figure 4). Typical configurations position a working electrode in close proximity to a gas-permeable membrane leading to a vacuum chamber that houses a mass spectrometer (Figure 4a,b). Volatile and gaseous products are pervaporated, enter the vacuum chamber, and are detected by mass spectrometry (Figure 4c). Alternatively, mass spectrometry on liquid phase products can directly inform catalyst or solvent stability,[107,108] but such operando techniques for liquid phase products are not yet widely available and have different operating principles that will not be considered here. Because mass spectrometry offers faster time resolution than most other analytical techniques, EC-MS is suitable for product measurement under transient conditions, such as the application of a potential step or sweep (Figure 4d). This capability is complementary to other time-resolved operando electrocatalytic techniques, like vibrational spectroscopy and X-ray absorption spectroscopy, which provide information about adsorbates and the electronic state of the catalyst material.[109−113] Because EC-MS uniquely resolves product masses, it is a particularly powerful tool for investigations that involve isotopically labeled species.

The major challenges for practitioners of EC-MS are: (1) the method is highly sensitive to trace impurities, (2) detection by mass spectrometry results in spurious artifacts and convoluted signals, (3) EC-MS calibration is subject to ionization chamber pressure and composition that vary widely among configurations and experiments, (4) specific cell geometries induce mass transport and current inhomogeneities, and (5) the time distribution resulting from species traveling along slightly different paths from electrode to detector must be considered for dynamic measurements. Modern EC-MS systems are sensitive to pmol s^{-1} of product evolution, meaning trace impurities will be readily observed and can lead to data misinterpretation. Even in high purity aqueous electrolytes, this manifests in the detection of CO_2 at oxidative potentials, which results from the oxidation of unavoidable hydrocarbon impurities, especially on Pt electrodes. Organic impurities are difficult to remove from electrolytes, and while all techniques discussed thus far are sensitive to impurities that impact the electrochemical behavior, EC-MS measurements are particularly sensitive to trace quantities, thus requiring rigorous benchmarking of such background impurity signals. Electron ionization of product mixtures can fragment

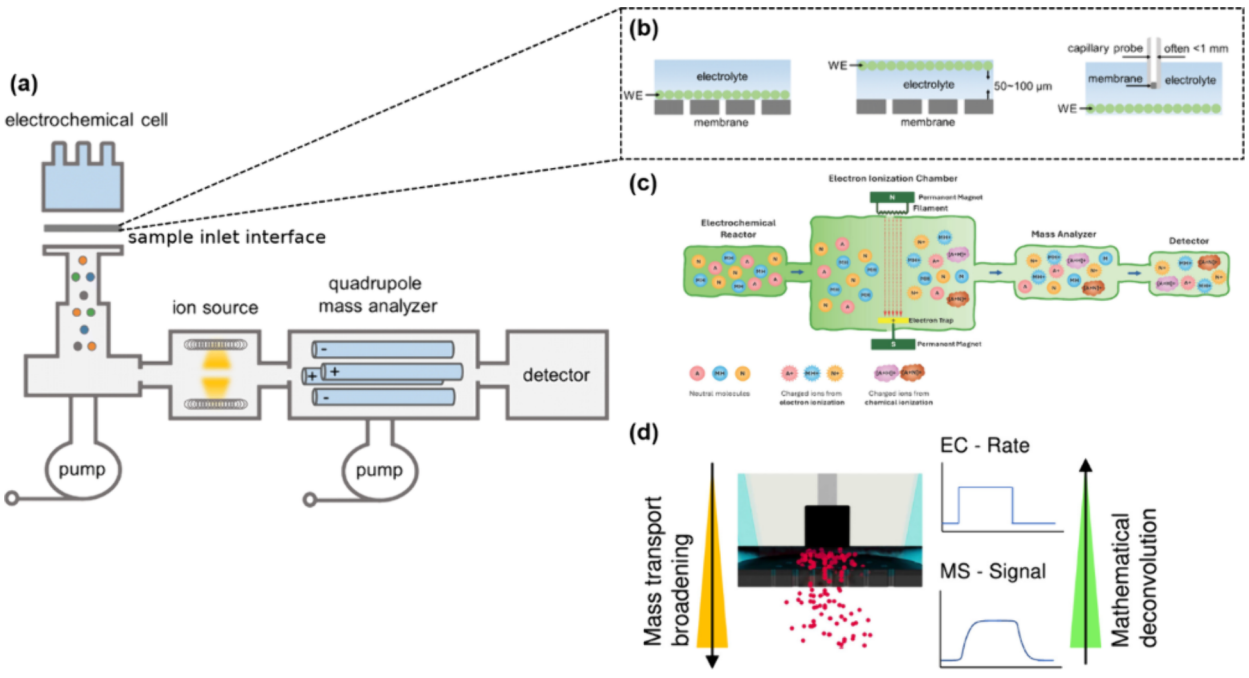

Figure 4. (a) Schematic diagram of a typical electrochemical mass spectrometer apparatus. Adapted from ref 114. Copyright 2024 Royal Society of Chemistry. (b) Examples of common inlet interface configurations for electrochemical mass spectrometry with the electrode placed directly on the interface membrane, positioned a short distance away from the membrane, or in a configuration where a small inlet membrane is fixed to capillary probe near the electrode. Adapted from ref 114. Copyright 2024 Royal Society of Chemistry. (c) Depiction of chemical reactions in the ionization chamber that can generate product detection inaccuracies. Reproduced from ref 115. Copyright 2025 American Chemical Society. (d) Depiction of signal broadening induced by mass transport effects in electrochemical mass spectrometry. Adapted from ref 116, licensed under CC-BY-NC-ND-4.0, https://creativecommons.org/licenses/by-nc-nd/4.0/.

https://doi.org/10.1021/acscatal.6c01946
ACS Catal. XXXX, XXX, XXX−XXX

dissimilar products into ions of the same m/z ratio, which represents a major challenge for determining the initial product concentration. In some cases, linear combinations of reference mass spectra can be used to deconvolute relative contributions from multiple species, but this generally requires knowledge of species identity and tends to be sensitive to drifts in mass spectrometer performance. Complementary product quantification methods may be required to fully attribute mass spectra of unknown product mixtures. Additionally, ionized fragments can undergo chemical reactions within the ionization chamber, leading to fragment masses that are unrelated to electrocatalytic processes. An understanding of fragment reactivity, combined with complementary product detection, is therefore essential for accurate EC-MS data interpretation. Further obstacles to data interpretation arise from the inherent difficulty of accurately calibrating mass spectrometers for the analysis of product concentrations. Product analysis in EC-MS takes place under significant partial pressures of solvent within the vacuum system and under varying chamber pressures that can (dynamically) influence analyte sensitivity. Accurate calibration and error estimation is thus critical for product quantification and faradaic efficiency estimation. Lastly, in some cell designs the close proximity of the working electrode to the permeable membrane induces significant inhomogeneities in mass and charge transport, which were already discussed in the section on Cross-Platform Challenges. Unique to electrochemical mass spectrometry, however, is the influence of cell geometry on the time required for species to travel from electrode to detector. Molecular diffusion within the electrochemical cell and in the vacuum system results in a distribution of travel times for species originating from a specific electrode process, resulting in signal broadening. This broadening needs to be considered if one wants to accurately relate the amount of product formed to the measured current, which typically requires performing a deconvolution of travel times. This is mathematically challenging and only possible for a limited set of experimental conditions.

Best practices to maintain rigor and reproducibility of EC-MS measurements start with awareness of the pitfalls described above. A series of recent publications address a subset of these challenges. A review by Yan highlights the most common contemporary EC-MS configurations, along with their typical applications and limitations.[114] Specific examples of operational practice for recently developed systems are provided by Clark and Trimarco.[117,118] Additionally, while the geometry of each apparatus is unique, a framework to evaluate the time delay between species generation at the electrode and its detection in the mass spectrometer was proposed by Krempl.[116] Lastly, Qiao critically assessed the formation of m/z signals unrelated to electrochemically generated analytes, concluding that such phenomena are highly system dependent, making reproducibility inherently challenging.[115] As such Qiao et al. propose to employ a series of careful benchmarking steps to identify species produced from reaction between fragments in the ionization chamber. We finally note that the methods, implementations, and applications of electrochemical mass spectrometry continue to face limitations but are rapidly evolving. Best practices and optimal operating conditions will likely be refined as EC-MS technology matures and its application widens. We encourage readers to actively contribute to this process and consider emerging literature to carry out EC-MS measurements with the highest degree of rigor and reproducibility.

Operando Electrochemical TEM

Operando electrochemical liquid-cell scanning/transmission electron microscopy (EC-TEM or EC-STEM) enables direct, nanoscale visualization of electrocatalyst structure and composition at the single-particle level under reactive liquid environments, providing insights that cannot be captured with bulk or ensemble techniques.[119−123] While conventional bright-field TEM, based on a parallel beam, is widely used to image light elements in biological samples,[124] scanning TEM (STEM) focuses an electron beam into a sub-Ångström probe and scans samples to acquire imaging, diffraction and spectroscopy-based signals analyzed by various detectors.[125] Imaging catalyst evolution in real time has proven especially powerful for nanostructured systems, which often undergo rapid morphological, structural and compositional changes during electrocatalytic operation. However, this capability comes with unusual constraints: the liquid environment must be confined within a sub-micrometer chamber to allow electron penetration, and electron doses must remain significantly lower than those used in conventional TEM images of dry samples to avoid undesired side reactions driven by beam-induced radiolytic species in liquids. Additionally, electrochemical control must be maintained so that measurements in the miniaturized liquid cell remain comparable to those performed in conventional electrochemical cells.[126] As with operando X-ray methods, thoughtful EC-STEM experimental design and transparent reporting are central to ensuring reproducible, interpretable results.

In the early 2000s, Ross and coworkers reported the first homebuilt in-situ liquid-cell TEM study of Cu electrodeposition.[127] Similar to the early liquid-cell, modern EC-STEM[127,128] employs a microelectromechanical-system (MEMS) liquid-cell composed of two thin SiN_x windows that enclose sub-μm of electrolyte, creating a sealed liquid environment stable under high vacuum (Figure 5a).[126,128−131] The pressure difference between the liquid-cell and ultra-high vacuum condition of TEM column leads to window bulging, increasing the effective liquid thickness, which further reduces spatial resolution and modifies electron scattering conditions. This architecture imposes fundamental limits on spatial resolution, which is governed not by the instrumental resolution limits but by the maximum tolerable beam dose in liquids. While atomic resolution is routinely achieved in dry samples at $\approx 10^6$ e^-/nm^2 or higher, operando liquid-cell imaging typically uses a low beam dose of ≈1 to 10 e^-/nm^2 to avoid radiolysis-driven chemistry, bubble formation, and/or window damage. Because these parameters vary from chip to chip (leaving a need in the community for more refined chip production), and even throughout a single experiment, reproducibility is strengthened when users characterize thickness and beam dose limits across various batches of liquid cells.

Electrochemical control presents an additional layer of complexity. Early liquid-cell studies used two-electrode configurations, which have been proven to be able to simulate two-electrode battery operation. However, it is insufficient for catalyst studies because quantitative analysis is hindered by convoluted polarization from the working and counter/reference electrodes. Modern EC-STEM liquid cells employ integrated three-electrode microchips with patterned working electrodes (WE), a large-area counter electrode (CE) surrounding the working electrode, and a Pt pseudo-reference electrode (RE) (Figure 5b). The Pt reference electrode is central to establishing

https://doi.org/10.1021/acscatal.6c01946
ACS Catal. XXXX, XXX, XXX−XXX

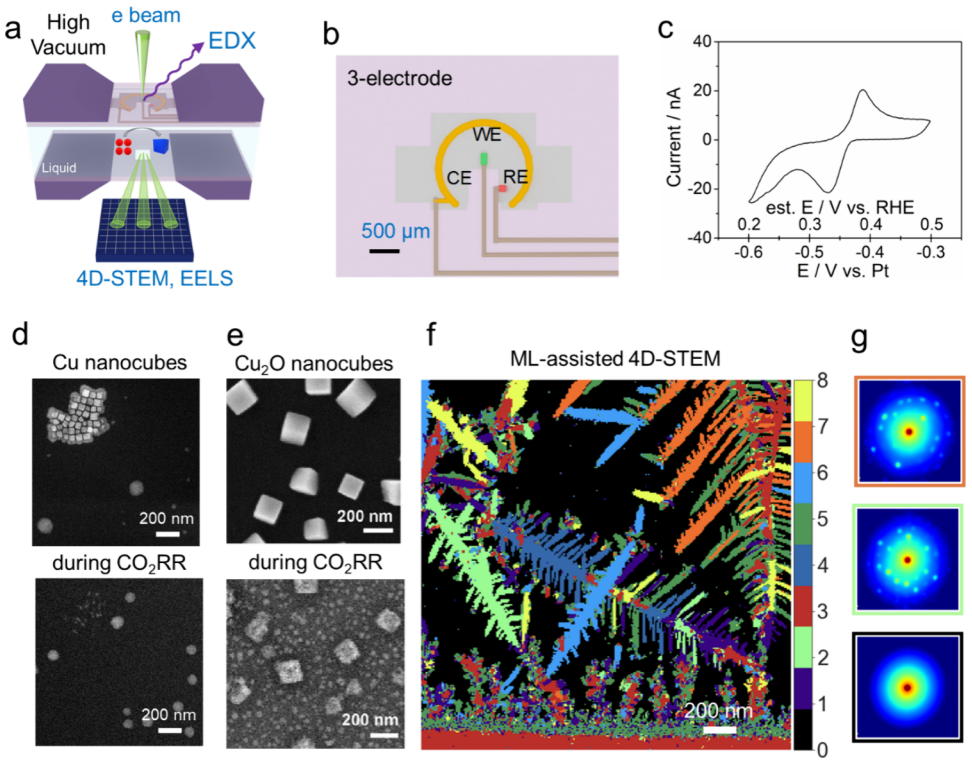

Figure 5. Operando/in situ electrochemical liquid-cell scanning/transmission electron microscopy (EC-S/TEM) for time-resolved nanoscale electrochemistry. (a) Schematic of the EC-STEM liquid cell encapsulated by two SiN_x windows, which enables quantitative electrochemistry (b) three-electrode EC-STEM electrochemical microchip with a large circular CE surrounding the WE and a Pt pseudo-RE. (c) CV profiles at 100 mV s^{-1} of Cu nanocatalysts supported on a glassy carbon WE using a EC-STEM liquid cell and in CO_2 saturated 0.1 mol L^{-1} $KHCO_3$ with a Pt RE that was converted to an estimated RHE scale. Operando EC-STEM images showing dynamic evolution of Cu (d) and Cu_2O (e) nanocubes during CO_2RR, respectively. Machine-learning-assisted 4D-STEM structural mapping of polycrystalline Cu dendrites (f) and representative electron diffraction patterns (g) corresponding to the numbers 0, 2, and 7 in (f) based on *k*-means hierarchical clustering. (a–c) Reproduced from ref 129. Copyright 2023 American Chemical Society. (d) is adapted with permission from ref 132. Copyright 2025 Springer Nature. (e) is adapted from ref 133. Available under a CC-BY 4.0 license (https://creativecommons.org/licenses/by/4.0/). Copyright 2021 P. Grosse, A. Yoon, C. Rettenmaier, A. Herzog, S. W. Chee, B. Roldan Cuenya. (f, g) Reproduced from ref 25. Copyright 2025 American Chemical Society.

an operando reference point of potential, yet remains one of the primary sources of uncertainty. Its potential is known to vary with pH, degree of surface oxide formation, and temperature. Comparisons of Pt electrode potentials with benchtop Ag/AgCl or reversible hydrogen reference electrodes show batch-dependent uncertainties on the order of ≈100 mV.[21] Figure 5c exhibits an example of a Cu^+/Cu redox couple in pH neutral CO_2 saturated 0.1 mol L^{-1} $KHCO_3$ during a CV measurement of Cu nanocatalysts.[134] Although this level of error may be tolerable for reactions with large overpotentials—such as oxygen evolution or CO_2 reduction—it is insufficient for reactions that are highly sensitive to potential, such as hydrogen evolution/oxidation or Li deposition. Accordingly, rigorous EC-STEM studies explicitly report reference calibration procedures, frequently using H_{UPD} features on Pt or well-defined redox couples such as Cu^{2+}/Cu,[135] as well as assessing temperature and pH dependent shifts in the Pt pseudo-RE.[25]

Beam-induced effects represent another major challenge to rigor, as 100–300 keV electron irradiation generates solvated electrons and radicals that can alter catalyst structures or local chemistry, even at low doses. EC-STEM therefore requires systematic beam-on/beam-off control experiments to confirm that imaging does not introduce spurious electrochemical signatures or morphological changes. Gas evolution compounds these issues. Radiolysis or electrocatalytic reactions routinely produce bubbles that modify local liquid thickness.[136] While bubble-induced thinning can sometimes improve spatial resolution, it also perturbs the electrochemical environment. Reproducibility demands explicit reporting of whether imaging was performed in "as-assembled thick liquid" or "thin liquid" conditions, as these regimes differ substantially in beam scattering, local resistance, and mass transport.[136]

Despite extreme confinement in scale, several studies have shown that mass transport near the working electrode can, under appropriate conditions, resemble bulk diffusion behavior. For example, $Fe(CN)_6^{3-}$/ $Fe(CN)_6^{4-}$ redox kinetics measured at various scan rates in EC-STEM yield diffusion coefficients comparable to benchtop measurements.[126] This agreement likely arises because both the electrode dimensions and electrolyte thickness scale down together, preserving the ratio between diffusion length and electrode size. Nonetheless, the ultramicroelectrode-like WE geometry means that even small obstructions—such as bubble formation at the counter electrode or restricted electrolyte pathways—can cause significant mass-transport artifacts. Reporting electrolyte geometry, diffusion pathway length, and any flow conditions is therefore essential for reproducibility.

https://doi.org/10.1021/acscatal.6c01946
ACS Catal. XXXX, XXX, XXX–XXX

Because the liquid volume near the working electrode is only on the picoliter-level, reaction products formed during EC-STEM experiments cannot be detected directly by mass spectrometry, or spectroscopy. Thus, rigorous operando studies must be benchmarked against parallel benchtop electrochemical measurements. These comparisons should verify that redox features, catalyst evolution pathways, and steady-state catalytic behaviors are consistent across the two environments. EC-STEM experiments often monitor structural changes—such as the transformation of Cu and Cu_2O nanocubes into polycrystalline metallic nanoscale grains (Figure 5d,e)[25,132,133]—on timescales of seconds or minutes whereas benchtop experiments can take place over hours. Such discrepancies underscore that strong electric fields in thin electrolyte layers accelerate certain electrochemical processes, and that operando interpretations must be cross-validated with macroscale experiments step by step.

A major strength of EC-STEM is its access to multi-modal structural and chemical information beyond imaging. Electrogenerated gas bubbles often reduce the liquid layer to ≈100 nm, enabling four-dimensional-STEM (4D-STEM) diffraction mapping,[136] energy dispersive X-ray spectroscopy (EDX)[137] or electron energy loss spectroscopy (EELS) elemental analysis.[128,138] 4D-STEM acquires a 2D STEM image in real space and simultaneous 2D electron diffraction in reciprocal space at each pixel of the image.[139,140] Advances in direct electron detectors allow gigabyte-scale 4D-STEM datasets to be collected within minutes, capturing grain-boundary formation, crystallographic orientation, and morphological transitions with nanometer resolution. 4D-STEM reveals the formation of μm-sized Cu dendrites with preferential crystallographic orientation on top of the granular Cu nanostructures in thin liquids (Figure 5f) based on machine-learning-assisted clustering of various electron diffraction patterns (Figure 5g). Machine-learning workflows are increasingly essential for analyzing these gigabyte-to-terabyte-level datasets and identifying robust, reproducible structural fingerprints. These techniques can be powerful when tightly coupled to well-calibrated electrochemistry—but require strict control of dose, acquisition time, and beam-induced chemistry—highlighting that although operando EC-STEM uniquely resolves nanoscale catalyst evolution with high temporal and spatial resolution, its inherent constraints demand rigorous controls and systematic validation against benchtop electrochemistry for quantitative, reproducible interpretation alongside complementary operando probes.[141]

■ CONCLUSION AND OUTLOOK

The continued expansion of operando electrocatalytic methods has fundamentally reshaped how catalytic interfaces are interrogated under working conditions. Yet, as emphasized throughout this Perspective, the power of these techniques is jeopardized by their susceptibility to misinterpretation when experimental rigor, validation, and transparent reporting are not prioritized. Across X-ray/vibrational spectroscopies, mass spectrometry, and electron microscopy platforms, recurring challenges—mass transport limitations, non-uniform current distribution, temporal mismatches, auxiliary electrode artifacts, catalyst evolution, and probe-induced effects—emerge regardless of the specific modality. Addressing these issues is therefore not a technique-specific exercise, but a unifying metrological imperative.

Moving forward, the most robust operando studies will increasingly rely on multimodal integration and cross-validation, rather than isolated measurements. Correlating surface-sensitive vibrational signatures with electronic and structural descriptors from X-ray spectroscopies, or pairing nanoscale imaging with quantitative product detection, provides a pathway to discriminate true catalytic phenomena from experimental artifacts. Such integration also imposes a higher bar for experimental design: electrochemical performance must be benchmarked against conventional cells, synchronization protocols (e.g., governing the timing and alignment of electrochemical stimuli, spectroscopic/imaging acquisition, and product analysis) must be explicit, and assumptions inherent to each technique must be openly acknowledged. In a similar way, the impact of emerging operando methodologies[142−146] will be increasingly contingent on rigorous experimental design, validation, and reporting practices, including the general reporting checklist provided in the Supporting Information.

Ultimately, advancing rigor and reproducibility in operando electrocatalysis will depend as much on community behavior as on technical innovation. Greater willingness to share cell designs, operational constraints, calibration procedures, and negative results would substantially lower barriers to reproducibility across laboratories. In parallel, the establishment of community-curated repositories, including reference spectra acquired under well-defined electrochemical conditions, benchmark datasets that link electrochemical performance to structural or spectroscopic observables, and fully documented operando protocols (cell geometry, electrode preparation, calibration procedures, and transport conditions), would provide a durable foundation for cross-platform comparison and independent validation.

By consistently applying operando techniques as quantitative measurements rather than relying on qualitative or correlative interpretation alone, and by embedding rigor, transparency, and cross-validation into their routine use, the electrocatalysis community can ensure that operando insights translate into reproducible mechanistic understanding and, ultimately, into reliable guidance for catalyst design. We hope this Perspective serves both as a practical reference and as an invitation for continued collective effort toward a shared metrological framework for operando electrochemistry.

■ ASSOCIATED CONTENT

Supporting Information

The Supporting Information is available free of charge at https://pubs.acs.org/doi/10.1021/acscatal.6c01946.

Best-practice checklist for reporting operando electrocatalytic measurements, including guidance for cell design and transport environment, electrochemical characterization, working-electrode preparation and stability, technique-specific measurement conditions, calibration and quantification, spectral and signal assignment, and benchmarking and cross-validation (DOCX)

■ AUTHOR INFORMATION

Corresponding Authors

Brian M. Tackett – *Davidson School of Chemical Engineering, Purdue University, West Lafayette, Indiana 47907, United States;* orcid.org/0000-0002-5996-5339;
Email: bmtacket@purdue.edu

https://doi.org/10.1021/acscatal.6c01946
ACS Catal. XXXX, XXX, XXX−XXX

Evan P. Jahrman – *Material Measurement Laboratory, National Institute of Standards and Technology, Gaithersburg, Maryland 20899, United States;* orcid.org/0000-0002-9590-0057; Email: evan.jahrman@nist.gov
Matthias M. Waegele – *Department of Chemistry, Merkert Chemistry Center, Boston College, Chestnut Hill, Massachusetts 02467, United States;* orcid.org/0000-0002-1186-7545; Email: waegele@bc.edu
Yao Yang – *Department of Chemistry and Chemical Biology, Cornell University, Ithaca, New York 14853, United States;* orcid.org/0000-0003-0321-3792; Email: yaoyang@cornell.edu
David Raciti – *Material Measurement Laboratory, National Institute of Standards and Technology, Gaithersburg, Maryland 20899, United States;* orcid.org/0000-0002-9580-4524; Email: david.raciti@nist.gov

Authors

Marcel Schreier – *Department of Chemical and Biological Engineering, University of Wisconsin–Madison, Madison, Wisconsin 53706, United States;* orcid.org/0000-0002-3674-5667
Ezra L. Clark – *Department of Chemical Engineering, The Pennsylvania State University, University Park, Pennsylvania 16802, United States;* orcid.org/0000-0002-0435-1276
Linsey C. Seitz – *Department of Chemical and Biological Engineering, Northwestern University, Evanston, Illinois 60208, United States;* orcid.org/0000-0001-6831-6747
Adam S. Hoffman – *SSRL, SLAC National Accelerator Laboratory, Menlo Park, California 94025, United States;* orcid.org/0000-0002-7682-4108
Qiaowan Chang – *The Gene and Linda Voiland School of Chemical Engineering and Bioengineering, Washington State University, Pullman, Washington 99164, United States;* orcid.org/0000-0003-1765-2331
Simon R. Bare – *SSRL, SLAC National Accelerator Laboratory, Menlo Park, California 94025, United States;* orcid.org/0000-0002-4932-0342
Jingguang G. Chen – *Department of Chemical Engineering, Columbia University, New York City, New York 10027, United States;* orcid.org/0000-0002-9592-2635
Elizabeth R. Corson – *Department of Chemical and Petroleum Engineering, University of Kansas, Lawrence, Kansas 66045, United States;* orcid.org/0000-0003-2722-674X
Anthony Shoji Hall – *Department of Materials Science and Engineering, University of Pennsylvania, Philadelphia, Pennsylvania 19104-6272, United States;* orcid.org/0000-0003-4134-4160
Sungin Kim – *Department of Chemistry and Chemical Biology, Cornell University, Ithaca, New York 14853, United States;* orcid.org/0000-0001-9107-0781
Jiahong Jiang – *Department of Chemistry and Chemical Biology, Cornell University, Ithaca, New York 14853, United States;* orcid.org/0009-0004-8750-2560

Complete contact information is available at: https://pubs.acs.org/doi/10.1021/acscatal.6c01946

Notes

Certain commercial equipment, instruments, software, or materials are identified in this paper to specify the experimental procedure adequately. Such identification is not intended to imply recommendation or endorsement by the National Institute of Standards and Technology, nor is it intended to imply that the materials or equipment identified are necessarily the best available for the purpose.
The authors declare no competing financial interest.

■ ACKNOWLEDGMENTS

This work was supported by the National Science Foundation through the Rigor and Reproducibility (R&R) program under Award No. CBET-2525020. This work used beamlines 6-BM and 7-ID-1 of the National Synchrotron Light Source II, a U.S. Department of Energy (DOE) Office of Science User Facility operated for the DOE Office of Science by Brookhaven National Laboratory under Contract No. DE-SC0012704. Y. Yang acknowledges the support from the National Science Foundation CAREER Award (2544087).

■ REFERENCES

(1) Yang, Y.; Xiong, Y.; Zeng, R.; Lu, X.; Krumov, M.; Huang, X.; Xu, W.; Wang, H.; DiSalvo, F. J.; Brock, J. D.; Muller, D. A.; Abruña, H. D. Operando Methods in Electrocatalysis. *ACS Catal.* **2021**, *11* (3), 1136–1178.
(2) Kolmeijer, K. E.; Mom, R. V. *Operando* Methods for the Elucidation of Electrolyte Effects in Electrocatalysis. *Curr. Opin. Electrochem.* **2025**, *51*, 101700.
(3) Prajapati, A.; Hahn, C.; Weidinger, I. M.; Shi, Y.; Lee, Y.; Alexandrova, A. N.; Thompson, D.; Bare, S. R.; Chen, S.; Yan, S.; Kornienko, N. Best Practices for In-Situ and Operando Techniques within Electrocatalytic Systems. *Nat. Commun.* **2025**, *16* (1), 2593.
(4) Akbashev, A. R. Electrocatalysis Goes Nuts. *ACS Catal.* **2022**, *12* (8), 4296–4301.
(5) Smith, G.; Dickinson, E. J. F. Error, Reproducibility and Uncertainty in Experiments for Electrochemical Energy Technologies. *Nat. Commun.* **2022**, *13* (1), 6832.
(6) Hausmann, J. N.; Pare, C. W. P.; Bagchi, D.; He, R.; Kaur, S.; Kumar, D.; Kwon, J.; Li, Z.; Walsh, M.; Wang, X.; Yang, R.; Zhao, Y.; Cabot, A.; Chen, Z.; Ha, Y.; Indra, A.; Kang, Z.; Nagaiah, T. C.; Patzke, G. R.; Pitchaimuthu, S.; Reuter, K.; Scheurer, C.; Schlatmann, R.; Song, T.; Sontheimer, T.; Wang, J.; Driess, M.; Menezes, P. W. Reproducibility in Electrocatalysis *ChemRxiv* **2025**.
(7) Sharifi Golru, S.; Biddinger, E. J. Influence of Electric Field and Current Distribution Due to Electrode Geometry on CO_2 Electroreduction. *Energy Fuels* **2024**, *38* (8), 7049–7056.
(8) Newman, J.; Thomas-Alyea, K. E. *Electrochemical Systems*, rd ed.; Electrochemical Society Series; Wiley-Interscience: Hoboken, NJ, **2004**.
(9) West, A. C. Electrochemistry and Electrochemical Engineering: An Introduction; Columbia University: New York, **2013**.
(10) Fogler, H. S. *Elements of Chemical Reaction Engineering*, th ed.; Pearson: Boston, **2020**.
(11) Son, Y. J.; Marquez, R. A.; Kawashima, K.; Smith, L. A.; Chukwuneke, C. E.; Babauta, J.; Mullins, C. B. Navigating iR Compensation: Practical Considerations for Accurate Study of Oxygen Evolution Catalytic Electrodes. *ACS Energy Lett.* **2023**, *8* (10), 4323–4329.
(12) Wagner, C. Theoretical Analysis of the Current Density Distribution in Electrolytic Cells. *J. Electrochem. Soc.* **1951**, *98* (3), 116.
(13) Kim, K. R.; Kim, S. K.; Kim, J. G.; Nam, H. O. CFD Approach to Wagner Number Estimation for a Current Distribution Uniformity in a Rotating Cylinder Hull Cell. *Int. J. Electrochem. Sci.* **2018**, *13* (9), 8686–8693.
(14) Inzelt, G.; Lewenstam, A.; Scholz, F. *Handbook of Reference Electrodes*; Springer Berlin Heidelberg: Berlin, Heidelberg, **2013**.

(15) Gamry Instruments. Improving Potentiostat Stability. https://www.gamry.com/support-2/technical-support/frequently-asked-questions/improving-potentiostat-stability/ (accessed 2025-12-30).
(16) Brett, C. M. A.; Brett, A. M. O. *Electrochemistry: Principles, Methods, and Applications*; Oxford University Press: Oxford, New York, **1993**.
(17) Bard, A. J.; Faulkner, L. R.; White, H. S. *Electrochemical Methods: Fundamentals and Applications*; John Wiley & Sons, **2022**.
(18) Wakelin, T. S. A.; Smith, G.Potential Potential Uncertainty – Understanding Uncertainty in Reference Electrode Measurements *ECS Meet. Abstr.* **2025** *MA2025-02*, 3440.
(19) Covington, A. K.; Whalley, P. D.; Davison, W. Recommendations for the Determination of pH in Low Ionic Strength Fresh Waters. *Pure Appl. Chem.* **1985**, *57* (6), 877–886.
(20) Torriero, A. A. Understanding the Differences between a Quasi-Reference Electrode and a Reference Electrode. *Med. Anal. Chem. Int. J.* **2019**, *3* (3) 000144.
(21) Zhang, Z.; Kim, S.; Briega-Martos, V.; Kennedy, E. R.; Zeltmann, S. E.; Thiede, E. H.; Yang, Y. Benchmarking Nanoscale Electrochemistry in Operando Transmission Electron Microscopy with a Standard Reference Electrode. *Nano Lett.* **2026**, 26 (10), 3463–3470.
(22) Davies, B.; Garcia-Martinez, F.; Goodwin, C. M.; Degerman, D.; Soldemo, M.; Lömker, P.; Grigorev, V.; Bibi, S. B.; Ali-Löytty, H.; Engel, R. Y.; Stenlid, J. H.; Rodrigues, G. L. S.; Hansson, T.; Schlueter, C.; Zou, X.; Nilsson, A.; Koroidov, S. Insight into the Carbon Monoxide Reduction Reaction on Cu(111) from Operando Electrochemical X-Ray Photoelectron Spectroscopy. *Angew. Chem., Int. Ed.* **2025**, *64* (33), e202506402.
(23) Dunwell, M.; Yang, X.; Yan, Y.; Xu, B. Potential Routes and Mitigation Strategies for Contamination in Interfacial Specific Infrared Spectroelectrochemical Studies. *J. Phys. Chem. C* **2018**, *122* (43), 24658–24664.
(24) Merkens, S.; Tollan, C.; De Salvo, G.; Bejtka, K.; Fontana, M.; Chiodoni, A.; Kruse, J.; Iriarte-Alonso, M. A.; Grzelczak, M.; Seifert, A.; Chuvilin, A. Toward Sub-Second Solution Exchange Dynamics in Flow Reactors for Liquid-Phase Transmission Electron Microscopy. *Nat. Commun.* **2024**, *15* (1), 2522.
(25) Kim, S.; Briega-Martos, V.; Liu, S.; Je, K.; Shi, C.; Stephens, K. M.; Zeltmann, S. E.; Zhang, Z.; Guzman-Soriano, R.; Li, W.; Jiang, J.; Choi, J.; Negash, Y. J.; Walden, F. S. I.; Marthe, N. L., Jr.; Wellborn, P. S.; Guo, Y.; Damiano, J.; Han, Y.; Thiede, E. H.; Yang, Y. Operando Heating and Cooling Electrochemical 4D-STEM Probing Nanoscale Dynamics at Solid–Liquid Interfaces. *J. Am. Chem. Soc.* **2025**, *147* (27), 23654–23671.
(26) Seitz, L. C.; Doronkin, D. E.; Hauschild, D.; Casapu, M.; Zengel, D.; Zimina, A.; Kreikemeyer-Lorenzo, D.; Blum, M.; Yang, W.; Grunwaldt, J.-D.; Heske, C.; Weinhardt, L. Direct Observation of Reactant, Intermediate, and Product Species for Nitrogen Oxide-Selective Catalytic Reduction on Cu-SSZ-13 Using In Situ Soft X-Ray Spectroscopy. *J. Phys. Chem. C* **2022**, *126* (49), 20998–21009.
(27) Wang, J.; Hsu, C.-S.; Wu, T.-S.; Chan, T.-S.; Suen, N.-T.; Lee, J.-F.; Chen, H. M. In Situ X-Ray Spectroscopies beyond Conventional X-Ray Absorption Spectroscopy on Deciphering Dynamic Configuration of Electrocatalysts. *Nat. Commun.* **2023**, *14* (1), 6576.
(28) Wang, J.; Liu, M.-T.; Hsu, C.-S.; Chu, Y.-C.; Liao, Y.-F.; Pao, C.-W.; Chan, T.-S.; Chuang, W.-T.; Chen, J.-L.; Shao, Y.-C.; Ishii, H.; Hiraoka, N.; Chiang, C.-Y.; Chen, H. M.Resolving Dynamic Behavior of Electrocatalysts via Advances of Operando X-ray Absorption Spectroscopies: Potential Artifacts and Practical Guidelines. *Adv. Mater.*37, 182418797.
(29) Zang, J.; Ye, W.; Liu, Q.; Meng, J.; Yang, W. Plasmonic-Promoted Formation of Surface Adsorbed Stochastic CO during Electrochemical CO_2 and CO Reduction on Cu at Extreme Low Overpotentials. *J. Am. Chem. Soc.* **2025**, *147* (12), 10260–10267.
(30) Zhang, M.; Wang, R.; Cai, Z.-Y.; Zong, C.; Qiao, H.-T.; Wu, D.-Y.; Tian, Z.-Q. Electrochemical Surface-Enhanced Raman Spectroscopy for Energy Modulation of Surface Plasmon-Mediated Photoelectrochemical Reactions of Para-Aminothiophenol on Silver Nanoparticle-Modified Electrodes. *J. Phys. Chem. C* **2023**, *127* (46), 22590–22599.
(31) Maley, M.; Hill, J. W.; Saha, P.; Walmsley, J. D.; Hill, C. M. The Role of Heating in the Electrochemical Response of Plasmonic Nanostructures under Illumination. *J. Phys. Chem. C* **2019**, *123* (19), 12390–12399.
(32) Wang, J.; Huang, B.; Xiao, L.; Wang, G.; Zhuang, L. Operando Spectroscopic Insights into CO_2 Reduction at Electrode/Polyelectrolyte Interfaces. *Angew. Chem., Int. Ed.* *64*, e202509423.
(33) Li, Q.; Abruña, H. D. Device-Level Synchrotron-Based Operando Characterization of Electrochemistry at Scale. *Carbon Future* **2025**, *2* (4), 9200059.
(34) Ge, L.; Rabiee, H.; Li, M.; Subramanian, S.; Zheng, Y.; Lee, J. H.; Burdyny, T.; Wang, H. Electrochemical CO_2 Reduction in Membrane-Electrode Assemblies. *Chem* **2022**, *8* (3), 663–692.
(35) Volk, K.; Kreider, E.; Kwon, M.; Alia, S. Recent Progress in Understanding the Catalyst Layer in Anion Exchange Membrane Electrolyzers – Durability, Utilization, and Integration. *EES Catal.* **2024**, *2* (1), 109–137.
(36) Hursán, D.; Janáky, C. Operando Characterization of Continuous Flow CO_2 Electrolyzers: Current Status and Future Prospects. *Chem. Commun.* **2023**, *59* (11), 1395–1414.
(37) Groot, F. d. Multiplet Effects in X-Ray Spectroscopy. *Coord. Chem. Rev.* **2005**, *249* (1), 31–63.
(38) de Groot, F. M. F.; Fuggle, J. C.; Thole, B. T.; Sawatzky, G. A. 2p X-Ray Absorption of 3d Transition-Metal Compounds: An Atomic Multiplet Description Including the Crystal Field. *Phys. Rev. B* **1990**, *42* (9), 5459–5468.
(39) Al Samarai, M.; Hahn, A. W.; Beheshti Askari, A.; Cui, Y.-T.; Yamazoe, K.; Miyawaki, J.; Harada, Y.; Rüdiger, O.; DeBeer, S. Elucidation of Structure–Activity Correlations in a Nickel Manganese Oxide Oxygen Evolution Reaction Catalyst by Operando Ni L-Edge X-Ray Absorption Spectroscopy and 2p3d Resonant Inelastic X-Ray Scattering. *ACS Appl. Mater. Interfaces* **2019**, *11* (42), 38595–38605.
(40) Chen, J. G. NEXAFS Investigations of Transition Metal Oxides, Nitrides, Carbides, Sulfides and Other Interstitial Compounds. *Surf. Sci. Rep.* **1997**, *30* (1), 1–152.
(41) Calvin, S. *XAFS for Everyone*; CRC Press: Boca Raton, **2013**.
(42) Lee, I.; Lee, M.-S.; Tao, L.; Ikuno, T.; Khare, R.; Jentys, A.; Huthwelker, T.; Borca, C. N.; Kalinko, A.; Gutiérrez, O. Y.; Govind, N.; Fulton, J. L.; Hu, J. Z.; Glezakou, V.-A.; Rousseau, R.; Sanchez-Sanchez, M.; Lercher, J. A. Activity of Cu–Al–Oxo Extra-Framework Clusters for Selective Methane Oxidation on Cu-Exchanged Zeolites. *JACS Au* **2021**, *1* (9), 1412–1421.
(43) Bhowmick, A.; Srinivas, S.; Zhang, J.; Moncada, J.; Titus, C. J.; Ravel, B.; Jaye, C.; Fischer, D. A.; Yarema, G.; Luo, S.; Shu, Y.; Yu, K.; Warty, A.; Hwang, S.; Caratzoulas, S.; Vlachos, D. G.; Jahrman, E. P.; Liu, D. Active Sites in the Dealuminated Beta Zeolite-Supported Cobalt Catalyst for Non-Oxidative Ethane Dehydrogenation. *ACS Catal.* **2025**, *15* (12), 10372–10390.
(44) Li, R.; Nordlund, D.; Seitz, L. C. Material Dynamics of Manganese-Based Oxychlorides for Oxygen Evolution Reaction in Acid. *Chem. Mater.* **2024**, *36* (3), 1299–1307.
(45) Watts, B.; Thomsen, L.; Dastoor, P. C. Methods in Carbon K-Edge NEXAFS: Experiment and Analysis. *J. Electron Spectrosc. Relat. Phenom.* **2006**, *151* (2), 105–120.
(46) Guo, B.; Jamnuch, S.; Vinson, J.; Ravel, B.; Jahrman, E. P.; Raciti, D.; Hall, A. S. Cu-Induced Redox Stabilization of Zn in Electrodeposited ϵ-$CuZn_4$ during CO_2 Electroreduction. *J. Electrochem. Soc.* **2026**, *173* (5), 054504.
(47) Weiland, C.; Jaye, C.; Quackenbush, N. F.; Gann, E.; Fu, Z.; Kirkland, J. P.; Karlin, B. A.; Ravel, B.; Woicik, J. C.; Fischer, D. A. NIST HAXPES at NSLS and NSLS-II. *Synchrotron Radiat. News* **2018**, *31* (4), 23–28.
(48) Weinhardt, L.; Steininger, R.; Kreikemeyer-Lorenzo, D.; Mangold, S.; Hauschild, D.; Batchelor, D.; Spangenberg, T.; Heske, C.

https://doi.org/10.1021/acscatal.6c01946
ACS Catal. XXXX, XXX, XXX–XXX

X-SPEC: A 70 eV to 15 keV Undulator Beamline for X-Ray and Electron Spectroscopies. *J. Synchrotron Radiat.* **2021**, *28* (2), 609–617.
(49) Lu, K.; Stern, E. A. Size Effect of Powdered Sample on EXAFS Amplitude. *Nucl. Instrum. Methods Phys. Res.* **1983**, *212* (1), 475–478.
(50) Parratt, L. G.; Hempstead, C. F.; Jossem, E. L. "Thickness Effect" in Absorption Spectra near Absorption Edges. *Phys. Rev.* **1957**, *105* (4), 1228–1232.
(51) Stern, E. A.; Kim, K. Thickness Effect on the Extended-x-Ray-Absorption-Fine-Structure Amplitude. *Phys. Rev. B* **1981**, *23* (8), 3781–3787.
(52) Ma, Q.; Moffitt, S. L.; Keane, D. T. A New Route to Obtain Fluorescence X-Ray Absorption Spectra of Compounds and to Remove the Self-Absorption Induced Nonlinearity in the Spectra. *J. Synchrotron Radiat.* **2022**, *29* (2), 470–479.
(53) Ravel, B. ATOMS: Crystallography for the X-Ray Absorption Spectroscopist. *J. Synchrotron Radiat.* **2001**, *8* (2), 314–316.
(54) Tröger, L.; Arvanitis, D.; Baberschke, K.; Michaelis, H.; Grimm, U.; Zschech, E. Full Correction of the Self-Absorption in Soft-Fluorescence Extended x-Ray-Absorption Fine Structure. *Phys. Rev. B* **1992**, *46* (6), 3283–3289.
(55) Booth, C. H.; Bridges, F. Improved Self-Absorption Correction for Fluorescence Measurements of Extended x-Ray Absorption Fine-Structure. *Phys. Scr.* **2005**, *2005* (T115), 202.
(56) Lee, S.-J.; Titus, C. J.; Alonso Mori, R.; Baker, M. L.; Bennett, D. A.; Cho, H.-M.; Doriese, W. B.; Fowler, J. W.; Gaffney, K. J.; Gallo, A.; Gard, J. D.; Hilton, G. C.; Jang, H.; Joe, Y. I.; Kenney, C. J.; Knight, J.; Kroll, T.; Lee, J.-S.; Li, D.; Lu, D.; Marks, R.; Minitti, M. P.; Morgan, K. M.; Ogasawara, H.; O'Neil, G. C.; Reintsema, C. D.; Schmidt, D. R.; Sokaras, D.; Ullom, J. N.; Weng, T.-C.; Williams, C.; Young, B. A.; Swetz, D. S.; Irwin, K. D.; Nordlund, D. Soft X-Ray Spectroscopy with Transition-Edge Sensors at Stanford Synchrotron Radiation Lightsource Beamline 10-1. *Rev. Sci. Instrum.* **2019**, *90* (11), 113101.
(57) Velasco-Vélez, J.-J.; Falling, L. J.; Bernsmeier, D.; Sear, M. J.; Clark, P. C. J.; Chan, T.-S.; Stotz, E.; Hävecker, M.; Kraehnert, R.; Knop-Gericke, A.; Chuang, C.-H.; Starr, D. E.; Favaro, M.; Mom, R. V. A Comparative Study of Electrochemical Cells for in Situ X-Ray Spectroscopies in the Soft and Tender x-Ray Range. *J. Phys. D: Appl. Phys.* **2021**, *54* (12), 124003.
(58) Blum, M.; Weinhardt, L.; Fuchs, O.; Bär, M.; Zhang, Y.; Weigand, M.; Krause, S.; Pookpanratana, S.; Hofmann, T.; Yang, W.; Denlinger, J. D.; Umbach, E.; Heske, C. Solid and Liquid Spectroscopic Analysis (SALSA)–a Soft x-Ray Spectroscopy Endstation with a Novel Flow-through Liquid Cell. *Rev. Sci. Instrum.* **2009**, *80* (12), 123102.
(59) Sherwin, C.; Celorrio, V.; Podbevsek, U.; Rigg, K.; Hodges, T.; Ibraliu, A.; Telfer, A. J.; McLeod, L.; Difilippo, A.; Corbos, E. C.; Zalitis, C.; Russell, A. E. An Optimised Cell for in Situ XAS of Gas Diffusion Electrocatalyst Electrodes. *ChemCatChem* **2024**, *16* (19), e202400221.
(60) Bras, W.; Myles, D. A. A.; Felici, R. When X-Rays Alter the Course of Your Experiments*. *J. Phys.: Condens. Matter* **2021**, *33* (42), 423002.
(61) Zabilska, A.; Clark, A. H.; Ferri, D.; Nachtegaal, M.; Kröcher, O.; Safonova, O. V. Beware of Beam Damage under Reaction Conditions: X-Ray Induced Photochemical Reduction of Supported VOx Catalysts during in Situ XAS Experiments. *Phys. Chem. Chem. Phys.* **2022**, *24* (36), 21916–21926.
(62) Leshchev, D.; Rakitin, M.; Luvizotto, B.; Kadyrov, R.; Ravel, B.; Attenkofer, K.; Stavitski, E. The Inner Shell Spectroscopy Beamline at NSLS-II: A Facility for in Situ and Operando X-Ray Absorption Spectroscopy for Materials Research. *J. Synchrotron Radiat.* **2022**, *29* (Pt 4), 1095–1106.
(63) Routh, P. K.; Redekop, E.; Prodinger, S.; Hoeven, J. E. S., van der; Lim, K. R. G.; Aizenberg, J.; Nachtegaal, M.; Clark, A. H.; Frenkel, A. I. Restructuring Dynamics of Surface Species in Bimetallic Nanoparticles Probed by Modulation Excitation Spectroscopy. *Nat. Commun.* **2024**, *15* (1), 6736.
(64) Müller, P.; Hermans, I. Applications of Modulation Excitation Spectroscopy in Heterogeneous Catalysis. *Ind. Eng. Chem. Res.* **2017**, *56* (5), 1123–1136.
(65) Dai, Y.; Gorey, T. J.; Anderson, S. L.; Lee, S.; Lee, S.; Seifert, S.; Winans, R. E. Inherent Size Effects on XANES of Nanometer Metal Clusters: Size-Selected Platinum Clusters on Silica. *J. Phys. Chem. C* **2017**, *121* (1), 361–374.
(66) Árnadóttir, L.; Bagger, A.; Bates, J. S.; Clark, E. L.; Hu, G.; Janik, M. J.; Singh, N.; Stuve, E.; Gunasooriya, G. T. K. K.; Warburton, R. E. Rigor & Reproducibility in Electrocatalysis: Integrating Theory and Experiment. *ChemRxiv* **2026**, 0506.
(67) Nascimento, D. R.; Govind, N. Computational Approaches for XANES, VtC-XES, and RIXS Using Linear-Response Time-Dependent Density Functional Theory Based Methods. *Phys. Chem. Chem. Phys.* **2022**, *24* (24), 14680–14691.
(68) Vinson, J.; Rehr, J. J.; Kas, J. J.; Shirley, E. L. Bethe-Salpeter Equation Calculations of Core Excitation Spectra. *Phys. Rev. B* **2011**, *83* (11), 115106.
(69) Cui, Z.; Xie, C.; Feng, X.; Becknell, N.; Yang, P.; Lu, Y.; Zhai, X.; Liu, X.; Yang, W.; Chuang, Y.-D.; Guo, J. Revealing the Size-Dependent d–d Excitations of Cobalt Nanoparticles Using Soft X-Ray Spectroscopy. *J. Phys. Chem. Lett.* **2017**, *8* (2), 319–325.
(70) Stavitski, E.; Groot, F. M. F., de The CTM4XAS Program for EELS and XAS Spectral Shape Analysis of Transition Metal L Edges. *Micron* **2010**, *41* (7), 687–694.
(71) Rehr, J. J.; Kas, J. J.; Vila, F. D.; Prange, M. P.; Jorissen, K. Parameter-Free Calculations of X-Ray Spectra with FEFF9. *Phys. Chem. Chem. Phys.* **2010**, *12* (21), 5503–5513.
(72) Meyer, R. J.; Bare, S. R.; Canning, G. A.; Chen, J. G.; Chu, P. M.; Hock, A. S.; Hoffman, A. S.; Karim, A. M.; Kelly, S. D.; Lei, Y.; Stavitski, E.; Wrasman, C. J. Recommendations to Standardize Reporting, Execution, and Interpretation of X-Ray Absorption Spectroscopy Measurements. *J. Catal.* **2024**, *432*, 115369.
(73) Rebstock, J. A.; Zhu, Q.; Baker, L. R. Exploring the Influence of Interfacial Solvation on Electrochemical CO_2 Reduction Using Plasmon-Enhanced Vibrational Sum Frequency Generation Spectroscopy. *ChemCatChem* **2024**, *16* (14), e202301301.
(74) Bhattacharyya, D.; Videla, P. E.; Palasz, J. M.; Tangen, I.; Meng, J.; Kubiak, C. P.; Batista, V. S.; Lian, T. Sub-Nanometer Mapping of the Interfacial Electric Field Profile Using a Vibrational Stark Shift Ruler. *J. Am. Chem. Soc.* **2022**, *144* (31), 14330–14338.
(75) Sorenson, S. A.; Patrow, J. G.; Dawlaty, J. M. Solvation Reaction Field at the Interface Measured by Vibrational Sum Frequency Generation Spectroscopy. *J. Am. Chem. Soc.* **2017**, *139* (6), 2369–2378.
(76) Kozuch, J.; Ataka, K.; Heberle, J. Surface-Enhanced Infrared Absorption Spectroscopy. *Nat. Rev. Methods Primer* **2023**, *3* (1), 70.
(77) Chen, S.; Meng, L.-Y.; Shan, H.-Y.; Li, J.-F.; Qian, L.; Williams, C. T.; Yang, Z.-L.; Tian, Z.-Q. How To Light Special Hot Spots in Multiparticle–Film Configurations. *ACS Nano* **2016**, *10* (1), 581–587.
(78) Paggi, L.; Fabas, A.; El Ouazzani, H.; Hugonin, J.-P.; Fayard, N.; Bardou, N.; Dupuis, C.; Greffet, J.-J.; Bouchon, P. Over-Coupled Resonator for Broadband Surface Enhanced Infrared Absorption (SEIRA). *Nat. Commun.* **2023**, *14* (1), 4814.
(79) Tseng, C.; Pennathur, A. K.; Blauth, D.; Salazar, N.; Dawlaty, J. M. Direct Determination of Plasmon Enhancement Factor and Penetration Depths in Surface Enhanced IR Absorption Spectroscopy. *Langmuir* **2023**, *39* (9), 3179–3184.
(80) Osawa, M. Surface-Enhanced Infrared Absorption. In *Near-Field Optics and Surface Plasmon Polaritons*; Kawata, S. , Ed.; Springer:Berlin, Heidelberg, **2001**, pp 163–187.
(81) Garcia-Araez, N.; Lukkien, J. J.; Koper, M. T. M.; Feliu, J. M. Competitive Adsorption of Hydrogen and Bromide on Pt(100): Mean-Field Approximation vs Monte Carlo Simulations. *J. Electroanal. Chem.* **2006**, *588* (1), 1–14.
(82) Bürgi, T. ATR-IR Spectroscopy at the Metal–Liquid Interface: Influence of Film Properties on Anomalous Band-Shape. *Phys. Chem. Chem. Phys.* **2001**, *3* (11), 2124–2130.

https://doi.org/10.1021/acscatal.6c01946
ACS Catal. XXXX, XXX, XXX–XXX

(83) Raciti, D.; Braun, T. M.; Hight Walker, A. R.; Moffat, T. P. Mapping Surface Chemistry During Superfilling with Shell-Isolated Nanoparticle Enhanced Raman Spectroscopy and X-Ray Photoelectron Spectroscopy. *J. Electrochem. Soc.* **2022**, *169*, 082506.
(84) Raciti, D.; Cockayne, E.; Vinson, J.; Schwarz, K.; Hight Walker, A. R.; Moffat, T. P. SHINERS Study of Chloride Order–Disorder Phase Transition and Solvation of Cu(100). *J. Am. Chem. Soc.* **2024**, *146* (2), 1588–1602.
(85) Salehi, M.; Schneider, L.; Ströbel, P.; Marx, A.; Packeisen, J.; Schlücker, S. Two-Color SERS Microscopy for Protein Co-Localization in Prostate Tissue with Primary Antibody–Protein A/G–Gold Nanocluster Conjugates. *Nanoscale* **2014**, *6* (4), 2361–2367.
(86) Dunwell, M.; Yan, Y.; Xu, B. A Surface-Enhanced Infrared Absorption Spectroscopic Study of pH Dependent Water Adsorption on Au. *Surf. Sci.* **2016**, *650*, 51–56.
(87) Wuttig, A.; Liu, C.; Peng, Q.; Yaguchi, M.; Hendon, C. H.; Motobayashi, K.; Ye, S.; Osawa, M.; Surendranath, Y. Tracking a Common Surface-Bound Intermediate during CO_2-to-Fuels Catalysis. *ACS Cent. Sci.* **2016**, *2* (8), 522–528.
(88) Chen, B.; Wijesinghe, M. S.; Hsu, Y.-S.; Zhang, R.; Gunathunge, C. M.; Grimaud, A.; Waegele, M. M. Avoiding Pitfalls in Probing Interfacial Solvation Structures Using Surface-Enhanced Infrared Absorption Spectroscopy. *J. Phys. Chem. C* **2026**, *130* (14), 5084–5093.
(89) Ye, W.; Yang, W. A Holistic View of Ions and Water Arrangements at the Electrified Cu Surface during Electrochemical CO_2 Conversion. *J. Phys. Chem. C* **2026**, *130* (1), 827–837.
(90) Hoffmann, F. M. Infrared Reflection-Absorption Spectroscopy of Adsorbed Molecules. *Surf. Sci. Rep.* **1983**, *3* (2), 107–192.
(91) Chang, S.-C.; Weaver, M. J. In-Situ Infrared Spectroscopy of CO Adsorbed at Ordered Pt(110)-Aqueous Interfaces. *Surf. Sci.* **1990**, *230* (1), 222–236.
(92) Moradzaman, M.; Mul, G. Infrared Analysis of Interfacial Phenomena during Electrochemical Reduction of CO_2 over Polycrystalline Copper Electrodes. *ACS Catal.* **2020**, *10* (15), 8049–8057.
(93) Miki, A.; Ye, S.; Osawa, M. Surface-Enhanced IR Absorption on Platinum Nanoparticles: An Application to Real-Time Monitoring of Electrocatalytic Reactions. *Chem. Commun.* **2002**, *14*, 1500–1501.
(94) Miyake, H.; Ye, S.; Osawa, M. Electroless Deposition of Gold Thin Films on Silicon for Surface-Enhanced Infrared Spectroelectrochemistry. *Electrochem. Commun.* **2002**, *4* (12), 973–977.
(95) Kraack, J. P.; Kaech, A.; Hamm, P. Surface Enhancement in Ultrafast 2D ATR IR Spectroscopy at the Metal-Liquid Interface. *J. Phys. Chem. C* **2016**, *120* (6), 3350–3359.
(96) Perakis, F.; De Marco, L.; Shalit, A.; Tang, F.; Kann, Z. R.; Kühne, T. D.; Torre, R.; Bonn, M.; Nagata, Y. Vibrational Spectroscopy and Dynamics of Water. *Chem. Rev.* **2016**, *116* (13), 7590–7607.
(97) Tackett, B. M.; Raciti, D.; Hight Walker, A. R.; Moffat, T. P. Surface Hydride Formation on Cu(111) and Its Decomposition to Form H_2 in Acid Electrolytes. *J. Phys. Chem. Lett.* **2021**, 10936–10941.
(98) Gunasekaran, P.; Du, X.; Burley, A.; Le, J.; Cheng, J.; Cuesta, A. Water at Electrode–Electrolyte Interfaces: Combining HOD Vibrational Spectra with Ab Initio-Molecular Dynamics Simulations. *Chem. Sci.* **2024**, *15* (42), 17469–17480.
(99) Sovago, M.; Campen, R. K.; Wurpel, G. W. H.; Müller, M.; Bakker, H. J.; Bonn, M. Vibrational Response of Hydrogen-Bonded Interfacial Water Is Dominated by Intramolecular Coupling. *Phys. Rev. Lett.* **2008**, *100* (17), 173901.
(100) Borguet, E.; Dai, H. Site-specific Properties and Dynamical Dipole Coupling of CO Molecules Adsorbed on a Vicinal Cu(100) Surface. *J. Chem. Phys.* **1994**, *101* (10), 9080–9095.
(101) Busson, B.; Tadjeddine, A. Non-Uniqueness of Parameters Extracted from Resonant Second-Order Nonlinear Optical Spectroscopies. *J. Phys. Chem. C* **2009**, *113* (52), 21895–21902.
(102) Pool, R. E.; Versluis, J.; Backus, E. H. G.; Bonn, M. Comparative Study of Direct and Phase-Specific Vibrational Sum-Frequency Generation Spectroscopy: Advantages and Limitations. *J. Phys. Chem. B.* **2011**, *115* (51), 15362–15369.
(103) Lagutchev, A.; Hambir, S. A.; Dlott, D. D. Nonresonant Background Suppression in Broadband Vibrational Sum-Frequency Generation Spectroscopy. *J. Phys. Chem. C* **2007**, *111* (37), 13645–13647.
(104) Lenk, T.; Schröder, U. An Experimental Guide to in Operando Electrochemical Raman Spectroscopy. *J. Solid State Electrochem.* **2024**, *28* (3), 965–979.
(105) Bell, J. S. E.; Sirimuthu, N. M. Quantitative Surface-Enhanced Raman Spectroscopy. *Chem. Soc. Rev.* **2008**, *37* (5), 1012–1024.
(106) Xu, Y.; Aljuhani, W.; Zhang, Y.; Ye, Z.; Li, C.; Bell, S. E. J. A Practical Approach to Quantitative Analytical Surface-Enhanced Raman Spectroscopy. *Chem. Soc. Rev.* **2025**, *54* (1), 62–84.
(107) Khanipour, P.; Löffler, M.; Reichert, A. M.; Haase, F. T.; Mayrhofer, K. J. J.; Katsounaros, I. Electrochemical Real-Time Mass Spectrometry (EC-RTMS): Monitoring Electrochemical Reaction Products in Real Time. *Angew. Chem., Int. Ed.* **2019**, *58* (22), 7273–7277.
(108) Löffler, M.; Khanipour, P.; Kulyk, N.; Mayrhofer, K. J. J.; Katsounaros, I. Insights into Liquid Product Formation during Carbon Dioxide Reduction on Copper and Oxide-Derived Copper from Quantitative Real-Time Measurements. *ACS Catal.* **2020**, *10* (12), 6735–6740.
(109) Li, Q.; Pollock, C. J.; Soto, J.; Villarino, A. M.; Shi, Z.; Krumov, M. R.; Muller, D. A.; Abruña, H. D. Operando X-Ray Absorption Spectroscopic Investigation of Electrocatalysts State in Anion Exchange Membrane Fuel Cells. *Nat. Commun.* **2025**, *16* (1), 3008.
(110) Ovalle, V. J.; Hsu, Y.-S.; Agrawal, N.; Janik, M. J.; Waegele, M. M. Correlating Hydration Free Energy and Specific Adsorption of Alkali Metal Cations during CO_2 Electroreduction on Au. *Nat. Catal.* **2022**, *5* (7), 624–632.
(111) Mariano, C. O. M.; Clemente, R. H.; Tsai, M.-H.; Chin, Y.-Y.; Chen, J.-M.; Lee, J.-F.; Lu, Y.-J.; Chen, C.-M.; Chen, P.-T.; Chuang, C.-H. Operando X-Ray and Mass Spectroscopy of Reduced Graphene Oxide (rGO)-Mediated Cobalt Catalysts for Boosting the Hydrogen Evolution Reaction. *PRX Energy* **2024**, *3* (3), 033005.
(112) Wang, H.; Abruña, H. D. Coupled Differential Electrochemical Mass Spectrometry and Surface-Enhanced Infrared Absorption Spectroscopic Studies Unravel the Mechanism of Nitric Oxide Electroreduction on Platinum. *J. Am. Chem. Soc.* **2025**, *147* (11), 9352–9364.
(113) Wang, H.; Abruña, H. D. New Insights into Methanol and Formic Acid Electro-Oxidation on Pt: Simultaneous DEMS and ATR-SEIRAS Study under Well-Defined Flow Conditions and Simulations of CO Spectra. *J. Chem. Phys.* **2022**, *156* (3), 034703.
(114) Zhao, K.; Jiang, X.; Wu, X.; Feng, H.; Wang, X.; Wan, Y.; Wang, Z.; Yan, N. Recent Development and Applications of Differential Electrochemical Mass Spectrometry in Emerging Energy Conversion and Storage Solutions. *Chem. Soc. Rev.* **2024**, *53* (13), 6917–6959.
(115) Qiao, Y.; Seger, B. Interesting Signals from Electrochemical Mass Spectrometry: Are They Real? Probably Not Chemical Ionization Can Distort Electron Ionization Mass Spectra. *ACS Electrochem.* **2025**, *1* (9), 1677–1686.
(116) Krempl, K.; Hochfilzer, D.; Scott, S. B.; Kibsgaard, J.; Vesborg, P. C. K.; Hansen, O.; Chorkendorff, I. Dynamic Interfacial Reaction Rates from Electrochemistry–Mass Spectrometry. *Anal. Chem.* **2021**, *93* (18), 7022–7028.
(117) Clark, E. L.; Singh, M. R.; Kwon, Y.; Bell, A. T. Differential Electrochemical Mass Spectrometer Cell Design for Online Quantification of Products Produced during Electrochemical Reduction of CO_2. *Anal. Chem.* **2015**, *87* (15), 8013–8020.
(118) Trimarco, D. B.; Scott, S. B.; Thilsted, A. H.; Pan, J. Y.; Pedersen, T.; Hansen, O.; Chorkendorff, I.; Vesborg, P. C. K. Enabling Real-Time Detection of Electrochemical Desorption Phenomena with Sub-Monolayer Sensitivity. *Electrochim. Acta* **2018**, *268*, 520–530.
(119) Ross, F. M. Opportunities and Challenges in Liquid Cell Electron Microscopy. *Science* **2015**, *350* (6267), aaa9886.

https://doi.org/10.1021/acscatal.6c01946
ACS Catal. XXXX, XXX, XXX–XXX

(120) Jonge, N., de; Ross, F. M. Electron Microscopy of Specimens in Liquid. *Nat. Nanotechnol.* **2011**, *6* (11), 695–704.
(121) Jonge, N., de; Houben, L.; Dunin-Borkowski, R. E.; Ross, F. M. Resolution and Aberration Correction in Liquid Cell Transmission Electron Microscopy. *Nat. Rev. Mater.* **2019**, *4* (1), 61–78.
(122) Yang, Y.; Feijóo, J.; Briega-Martos, V.; Li, Q.; Krumov, M.; Merkens, S.; De Salvo, G.; Chuvilin, A.; Jin, J.; Huang, H.; Pollock, C. J.; Salmeron, M. B.; Wang, C.; Muller, D. A.; Abruña, H. D.; Yang, P. *Operando* Methods: A New Era of Electrochemistry. *Curr. Opin. Electrochem.* **2023**, *42*, 101403.
(123) Vigil, S. A.; Lin, Z.; Moreno-Hernandez, I. A. Advancing Electrocatalyst Design Principles via Liquid-Phase Transmission Electron Microscopy. *ACS Catal.* **2025**, *15* (23), 19810–19822.
(124) Ruska, E. The Development of the Electron Microscope and of Electron Microscopy. *Biosci. Rep.* **1987**, *7* (8), 607–629.
(125) Muller, D. A. Structure and Bonding at the Atomic Scale by Scanning Transmission Electron Microscopy. *Nat. Mater.* **2009**, *8* (4), 263–270.
(126) Unocic, R. R.; Sacci, R. L.; Brown, G. M.; Veith, G. M.; Dudney, N. J.; More, K. L.; Walden, F. S., II; Gardiner, D. S.; Damiano, J.; Nackashi, D. P. Quantitative Electrochemical Measurements Using In Situ Ec-S/TEM Devices. *Microsc. Microanal.* **2014**, *20* (2), 452–461.
(127) Williamson, M. J.; Tromp, R. M.; Vereecken, P. M.; Hull, R.; Ross, F. M. Dynamic Microscopy of Nanoscale Cluster Growth at the Solid–Liquid Interface. *Nat. Mater.* **2003**, *2* (8), 532–536.
(128) Holtz, M. E.; Yu, Y.; Gunceler, D.; Gao, J.; Sundararaman, R.; Schwarz, K. A.; Arias, T. A.; Abruña, H. D.; Muller, D. A. Nanoscale Imaging of Lithium Ion Distribution During In Situ Operation of Battery Electrode and Electrolyte. *Nano Lett.* **2014**, *14* (3), 1453–1459.
(129) Yang, Y.; Shao, Y.-T.; Jin, J.; Feijóo, J.; Roh, I.; Louisia, S.; Yu, S.; Fonseca Guzman, M. V.; Chen, C.; Muller, D. A.; Abruña, H. D.; Yang, P. Operando Electrochemical Liquid-Cell Scanning Transmission Electron Microscopy (EC-STEM) Studies of Evolving Cu Nanocatalysts for CO_2 Electroreduction. *ACS Sustainable Chem. Eng.* **2023**, *11* (10), 4119–4124.
(130) Yang, Y.; Louisia, S.; Yu, S.; Jin, J.; Roh, I.; Chen, C.; Fonseca Guzman, M. V.; Feijóo, J.; Chen, P.-C.; Wang, H.; Pollock, C. J.; Huang, X.; Shao, Y.-T.; Wang, C.; Muller, D. A.; Abruña, H. D.; Yang, P. Operando Studies Reveal Active Cu Nanograins for CO_2 Electroreduction. *Nature* **2023**, *614* (7947), 262–269.
(131) Yang, Y.; Roh, I.; Louisia, S.; Chen, C.; Jin, J.; Yu, S.; Salmeron, M. B.; Wang, C.; Yang, P. Operando Resonant Soft X-Ray Scattering Studies of Chemical Environment and Interparticle Dynamics of Cu Nanocatalysts for CO_2 Electroreduction. *J. Am. Chem. Soc.* **2022**, *144* (20), 8927–8931.
(132) Yang, Y.; Feijóo, J.; Figueras-Valls, M.; Chen, C.; Shi, C.; Fonseca Guzman, M. V.; Murhabazi Maombi, Y.; Liu, S.; Jain, P.; Briega-Martos, V.; Peng, Z.; Shan, Y.; Lee, G.; Rebarchik, M.; Xu, L.; Pollock, C. J.; Jin, J.; Soland, N. E.; Wang, C.; Salmeron, M. B.; Chen, Z.; Han, Y.; Mavrikakis, M.; Yang, P. Operando Probing Dynamic Migration of Copper Carbonyl during Electrocatalytic CO_2 Reduction. *Nat. Catal.* **2025**, *8* (6), 579–594.
(133) Grosse, P.; Yoon, A.; Rettenmaier, C.; Herzog, A.; Chee, S. W.; Roldan Cuenya, B. Dynamic Transformation of Cubic Copper Catalysts during CO_2 Electroreduction and Its Impact on Catalytic Selectivity. *Nat. Commun.* **2021**, *12* (1), 6736.
(134) Walker, N. L.; Dick, J. E. Leakless, Bipolar Reference Electrodes: Fabrication, Performance, and Miniaturization. *Anal. Chem.* **2021**, *93* (29), 10065–10074.
(135) Yang, Y.; Shao, Y.-T.; DiSalvo, F. J.; Muller, D. A.; Abruña, H. D. Metal Monolayers on Command: Underpotential Deposition at Nanocrystal Surfaces: A Quantitative Operando Electrochemical Transmission Electron Microscopy Study. *ACS Energy Lett.* **2022**, *7* (4), 1292–1297.
(136) Yang, Y.; Shao, Y.-T.; Lu, X.; Yang, Y.; Ko, H.-Y.; DiStasio, R. A. J.; DiSalvo, F. J.; Muller, D. A.; Abruña, H. D. Elucidating Cathodic Corrosion Mechanisms with Operando Electrochemical Transmission Electron Microscopy. *J. Am. Chem. Soc.* **2022**, *144* (34), 15698–15708.
(137) Lewis, E. A.; Haigh, S. J.; Slater, T. J. A.; He, Z.; Kulzick, M. A.; Burke, M. G.; Zaluzec, N. J. Real-Time Imaging and Local Elemental Analysis of Nanostructures in Liquids. *Chem. Commun.* **2014**, *50* (70), 10019–10022.
(138) Holtz, M. E.; Yu, Y.; Gao, J.; Abruña, H. D.; Muller, D. A. In Situ Electron Energy-Loss Spectroscopy in Liquids. *Microsc. Microanal.* **2013**, *19* (4), 1027–1035.
(139) Tate, M. W.; Purohit, P.; Chamberlain, D.; Nguyen, K. X.; Hovden, R.; Chang, C. S.; Deb, P.; Turgut, E.; Heron, J. T.; Schlom, D. G.; Ralph, D. C.; Fuchs, G. D.; Shanks, K. S.; Philipp, H. T.; Muller, D. A.; Gruner, S. M. High Dynamic Range Pixel Array Detector for Scanning Transmission Electron Microscopy. *Microsc. Microanal.* **2016**, *22* (1), 237–249.
(140) Philipp, H. T.; Tate, M. W.; Shanks, K. S.; Mele, L.; Peemen, M.; Dona, P.; Hartong, R.; Veen, G., van; Shao, Y.-T.; Chen, Z.; Thom-Levy, J.; Muller, D. A.; Gruner, S. M. Very-High Dynamic Range, 10,000 Frames/Second Pixel Array Detector for Electron Microscopy. *Microsc. Microanal.* **2022**, *28* (2), 425–440.
(141) Choi, J.; Kim, S.; Choi, J. Y.; Park, S.; Je, K.; Liu, S.; Jiang, J.; Yang, S.; Pollock, C. J.; Guzman-Soriano, R.; Bairley, K.; Ahmad, B. I. Z.; Milner, P. J.; Thiede, E. H.; Hwang, Y. J.; Park, J.; Yang, Y. Dynamic Evolution from Single-Atom Catalysts to Active Nanograins for CO_2 Reduction. *J. Am. Chem. Soc.* **2025**, *147* (41), 37808–37818.
(142) Li, J.; Zhu, Q.; Chang, A.; Cheon, S.; Gao, Y.; Shang, B.; Li, H.; Rooney, C. L.; Ren, L.; Jiang, Z.; Liang, Y.; Feng, Z.; Yang, S.; Robert Baker, L.; Wang, H. Molecular-Scale CO Spillover on a Dual-Site Electrocatalyst Enhances Methanol Production from CO_2 Reduction. *Nat. Nanotechnol.* **2025**, *20* (4), 515–522.
(143) Dodin, A.; Deng, G.-H.; Rebstock, J. A.; Zhu, Q.; Limmer, D. T.; Baker, L. R. Sodium Carbonate Ion Complexes Modify Water Structure at Electrode Interfaces. *Appl. Surf. Sci.* **2024**, *667*, 160345.
(144) Zhu, Q.; Wallentine, S. K.; Deng, G.-H.; Rebstock, J. A.; Baker, L. R. The Solvation-Induced Onsager Reaction Field Rather than the Double-Layer Field Controls CO_2 Reduction on Gold. *JACS Au* **2022**, *2* (2), 472–482.
(145) Wallentine, S.; Bandaranayake, S.; Biswas, S.; Baker, L. R. Plasmon-Resonant Vibrational Sum Frequency Generation of Electrochemical Interfaces: Direct Observation of Carbon Dioxide Electroreduction on Gold. *J. Phys. Chem. A* **2020**, *124* (39), 8057–8064.
(146) Xu, P.; Wang, R.; Zhang, H.; Carnevale, V.; Borguet, E.; Suntivich, J. Cation Modifies Interfacial Water Structures on Platinum during Alkaline Hydrogen Electrocatalysis. *J. Am. Chem. Soc.* **2024**, *146* (4), 2426–2434.

https://doi.org/10.1021/acscatal.6c01946
ACS Catal. XXXX, XXX, XXX–XXX